AFRL-VS-TR-2003-1591

VALIDATION OF IONOSPHERIC MODELS

Patricia Doherty

Boston College
Institute for Scientific Research
140 Commonwealth Avenue
Chestnut Hill, MA 02467-3862

31 March 2000

Scientific Report No. 4

AIR FORCE RESEARCH LABORATORY
Space Vehicles Directorate
29 Randolph Rd
AIR FORCE MATERIEL COMMAND
Hanscom AFB, MA 01731-3010

"This technical report has been reviewed and is approved for publication"

/signed/

JOHN RETTERER
Contract Manager

/signed/

ROBERT MORRIS
Branch Chief

This report has been reviewed by the ESC Public Affairs Office (PA) and is releasable to the National Technical Information Service (NTIS).

Qualified requestors may obtain additional copies from the Defense Technical Information Center (DTIC). All others should apply to the National Technical Information Service (NTIS).

If your address has changed, if you wish to be removed from the mailing list, or if the addressee is no longer employed by your organization, please notify AFRL/VSIM, 29 Randolph Road, Hanscom AFB MA 01731-3010. This will assist us in maintaining a current mailing list.

Do not return copies of this report unless contractual obligations or notices on a specific document require that it be returned.

REPORT DOCUMENTATION PAGE

Form Approved
OMB No. 0704-0188

1. REPORT DATE *(DD-MM-YYYY)*	2. REPORT TYPE	3. DATES COVERED *(From - To)*
31-03-2000	Scientific Report No. 4	April 1999 - March 2000

4. TITLE AND SUBTITLE

VALIDATION OF IONOSPHERIC MODELS

5a. CONTRACT NUMBER
F19628-96-C-0039

5b. GRANT NUMBER

5c. PROGRAM ELEMENT NUMBER
61102F

6. AUTHOR(S)

Patricia H. Doherty

5d. PROJECT NUMBER
1010

5e. TASK NUMBER
IM

5f. WORK UNIT NUMBER
AC

7. PERFORMING ORGANIZATION NAME(S) AND ADDRESS(ES)

Boston College / Institute for Scientific Research
140 Commonwealth Avenue
Chestnut Hill, MA 02467-3862

8. PERFORMING ORGANIZATION REPORT NUMBER

9. SPONSORING/MONITORING AGENCY NAME(S) AND ADDRESS(ES)

Air Force Research Laboratory/VSBP
29 Randolph Road
Hanscom AFB, MA 01731-3010

10. SPONSOR/MONITOR'S ACRONYM(S)

11. SPONSOR/MONITOR'S REPORT NUMBER(S)
AFRL-VS-TR-2003-1591

12. DISTRIBUTION/AVAILABILITY STATEMENT

13. SUPPLEMENTARY NOTES

Approved for public release; distribution unlimited.

14. ABSTRACT

During the period of April 1999 through March 2000, research efforts continued in the Validation of Ionospheric Models. These efforts included the development and augmentation of a model that predicts positioning errors for the single-frequency GPS user. This model has the ability to utilize the Parameterized Ionosphere Model (PIM) or the Parameterized Real-time Ionosphere Model (PRISM). This model has further been assimilated into the Operational Space Environment Network Display (OP-SEND) space weather product. Other efforts included comprehensive validations of PIM and PRISM together with comparisons of PIM with other climatological models. Advancements were also made in the development of analytical techniques to theoretically model Equatorial Spread F. A database of TEC from the TOPEX satellite was accessed and used to describe longitudinal dependence of the equatorial anomaly and to test ExB control of the anomaly features of the LowLat model. Finally, efforts to define a relationship between rapid changes in TEC and amplitude scintillation were made.

15. SUBJECT TERMS

GPS, TEC, Positioning errors, PIM, PRISM, TOPEX, Scintillation

16. SECURITY CLASSIFICATION OF:			17. LIMITATION OF ABSTRACT	18. NUMBER OF PAGES	19a. NAME OF RESPONSIBLE PERSON
a. REPORT	b. ABSTRACT	c. THIS PAGE			John Retterer
U	U	U	SAR		19b. TELEPHONE NUMBER *(Include area code)* 781-377-3891

TABLE OF CONTENTS

1. GOALS

The objective of this contract is to obtain ionospheric measurements from a wide range of geographic locations and to utilize the resulting databases to validate the theoretical ionospheric models that are the basis of the Parameterized Ionospheric Specification Model (PRISM) and the Ionospheric Forecast Model (IFM).

In this past year, we have supported these goals with the following activities:

- improvement of the GPS positioning error map algorithms using PRISM.
- integration of the GPS positioning error map algorithms into the Operatioinal Space Environment Network Display.
- validations of the Parameterized Ionosphere Model (PIM) and the PRISM.
- the application of plasma kinetic equations for ionospheric modeling.
- studies of the longitudinal dependence of low-latitude TEC using the LOWLAT model.
- TEC and scintillation studies.

2. PROGRESS

2.1 Determination of Position Errors for Single-Frequency GPS Users

In last year's annual report, we described an initial effort to investigate navigational position errors caused by inaccuracies in the standard Ionospheric Correction Algorithm (ICA). The ICA is the only ionospheric correction available for single-frequency GPS users and it corrects for ~50 percent of the delay on pseudoranges introduced by the ionosphere. The residual delay, not accounted for by the ICA, can result in positioning errors for the single frequency GPS user. The work completed last year included the development of a set of algorithms that estimates the magnitude of those position errors and plots them on a worldwide map. These error estimates were determined by propagating the difference between the PIM ionospheric corrections and the ICA corrections through a series of complex position error equations. Last year's work included a limited validation of the method.

In the current year, work has continued on quantifying the magnitude of positioning errors that result from inadequate modeling of the ionosphere for single-frequency users. In particular, sensitivity studies were completed based on changes in solar activity and geographic location. Additionally, the algorithms were modified to provide more versatility in their use. These modifications included adding the ability to assimilate PRISM model output for ionospheric corrections and to allow the use of different types of satellite ephemeris sets. Finally, work was initiated to provide a more comprehensive validation of the algorithms.

This work resulted in three presentations and two papers in meeting proceedings.

In the current year, efforts were also made to integrate the position error maps into the OP-SEND. OP-SEND includes maps with near real-time estimates on:

- UHF SATCOM Scintillation
- HF Illumination
- Auroral Clutter Boundaries
- Scintillation Predictions
- GPS Single-Frequency Position Error

All of these components are useful in describing limitations for communication and navigation systems induced by the ionosphere.

2.2 Validations of the PIM and PRISM Models

A number of tasks were performed to aid the assessment and forecast of space environment conditions. Our prime contribution in these tasks was the validation efforts to establish operating performance baselines of the PIM and PRISM models.

Initial validations of PRISM were undertaken during 1999 at AFRL. PRISM was developed in the 1990's for operational use by the Air Force. The basic concept of PRISM is to use available ground-based and space-based data in near real-time to modify the physics-based climatological model (PIM) in order to provide a global specification of the ionosphere to higher accuracy than what climatology alone can provide. This validation effort was divided into two parts. One part focused on validating PRISM's climatology and the other part focused on the effectiveness of the real-time adjustment used by PRISM to adjust the PRISM climatology.

In the first effort, we compared PRISM's climatology to several datasets as well as several empirical ionospheric models. The datasets utilized in this work included Faraday Rotation TEC from four worldwide locations together with Defense Meteorological Satellite Program (DMSP) in-situ total ion density measurements. The models that were considered along with PRISM climatology were the Bent model, the International Reference Ionosphere (IRI), and the Raytrace/ICED, Bent, Gallagher model (RIBG). The overall results of these efforts were that model performance is quite variable. They all do a better job predicting TEC climatology at a mid-latitude location that they do the topside behavior as seen by DMSP. A sample of the results of this work is shown in Figure 1 where we display the RMS error averaged over a year during solar maximum. The RMS error was calculated by taking the difference between the value calculated by the model and an actual TEC measurement. Each panel in Figure 1 represents the comparison of the RMS errors for four different models for one station. Results for Hamilton, MA are shown in the left panel, while Taiwan and Ascension Island results are shown in the middle and right panels respectively. Note that the performance of the models is very similar with no big winners or losers in any location.

In the second effort, TOPEX TEC, GPS TEC and ground-based digisonde data was used to test PRISM's ability to produce an improved ionospheric specification over climatology. Initial runs of this effort showed that PRISM's ability to generate an improved ionospheric prediction is highly dependent on a particular location's distance from where the real-time observations are made. Further, there can be locations where the adjustments made in PRISM produce errors

larger than those of climatology. Efforts to quantify these errors and the conditions under which they occur will continue into the next year.

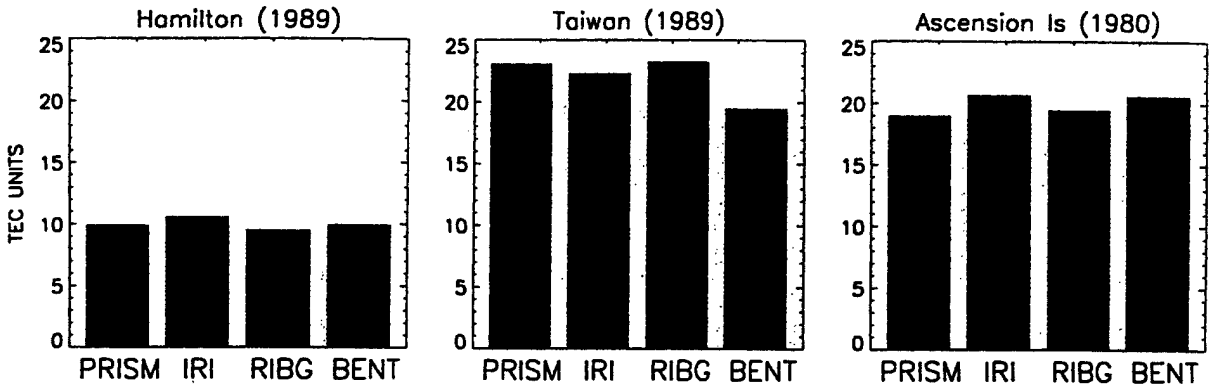

Figure 1. RMS Error Averaged Over a Year During Solar Maximum

2.3 Ionospheric Modeling Using Systems of Plasma Kinetic Equations

A physically accurate theoretical model of the Equatorial Spread F problem must include the variation of plasma perturbations along the Earth's curved geomagnetic field. Mathematically, this requires the solution of a second-order differential equation subject to the boundary conditions. A numerical code has been developed to solve the second-order differential equation, subject to the appropriate boundary conditions. This determines the Eigenvalue λ as well as the Eigenfunction ϕ. A positive, real value of λ indicates plasma instability. The validity of the numerical algorithm continues to be tested for different limiting cases of the differential equation, for which analytical solutions are known.

This work will continue in the next year with the goal to develop a theoretical model of equatorial spread F.

2.4 Longitudinal Evaluation of Low-Latitude TEC

The longitude structure of ionospheric TEC at low latitudes has been evaluated using the TOPEX/Poseidon satellite. The TEC data set illustrated patterns of longitudinal dependence of the equatorial anomaly during the equinoxes, summers and winters of 1993, 1994 and 1995. The TOPEX observations revealed occurrence of relative maximum anomaly TEC values in the Indian/Asian longitude sector. This dominance was seen most consistently in the Asian Southern Hemisphere. Also a relative decrease in anomaly TEC were evident in the western American region, which was primarily observed during the equinox and winter months.

The TOPEX data was further utilized in conjunction with the low latitude theoretical model to determine the dependence of anomaly features on ExB vertical drift velocities. This effort included attempts to reproduce the anomaly features of the TOPEX data by varying the strength of the ExB drift velocities. Results showed that ExB drift velocities were a primary factor in the longitudinal dependence of equatorial anomaly TEC. A summary of these efforts are contained in the paper "Longitude Structure of Ionospheric TEC at Low Latitude Measured by the

TOPEX/Poseidon Satellite," by J.A. Vladimer, P. Jastrzebski, M.C. Lee, P.H. Doherty, D.T. Decker and D.N. Anderson. A copy of this paper is appended to this report (see Appendix A).

2.5 TEC and Scintillation Studies

A study was initiated to determine the relationship between rapid changes in TEC and amplitude scintillation. Dual-frequency GPS TEC and amplitude scintillation measurements recorded at Ascension Island in the February-April 1998 time period were utilized. The reason for the study was to determine if rapid changes in TEC could be used as a proxy for amplitude scintillation. The results illustrated a strong correlation during the pre-midnight period and a poor correlation in the post-midnight period. S. Basu, K.M. Groves, J.M. Quinn and P. Doherty present a summary of this work in the paper, "A Comparison of TEC fluctuations and scintillations at Ascension Island." A copy of this paper is appended to this report (see Appendix B).

3. PRESENTATIONS

The work described in this report resulted in 12 oral presentations at various scientific meetings.

Decker, D.T., Wise, J.O., Borer, W.S., Daniell, R.E., and Doherty, P.H., "Validation of PRISM: Real Time Specification," presented at the 1999 Ionospheric Effects Symposium, Alexandria VA, May 1999.

Doherty, P.H., Decker, D.T., Sultan, P.J., Rich, F.J., Borer, W.S., and Daniell, R.E., "VValidation of PRISM: The Climatology V," presented at 1999 Ionospheric Effects Symposium, Alexandria VA, May 1999.

Smitham, M.C., Doherty, P.H., Delay, S.H., and Bishop, G.J., "VDetermination of Position Errors for Single-Frequency GPS ReceiversV," presented at the 1999 Ionospheric Effects Symposium, Alexandria VA, May 1999.

Doherty, P.H., Smitham, M.C., Delay, S.H., and Bishop, G.J., "VDetermination of Position Errors for Single-Frequency GPS ReceiversV," presented at the Institute of Navigation Annual Meeting, Cambridge MA, June 1999.

Decker, D.T., Doherty, P.H., Sultan, P.J., Rich, F.J., Borer, W.S., and Daniell, R.E., "VValidation of Ionospheric Models: The ClimatologyV," presented at the GIFT workshop at the CEDAR Meeting, Boulder CO, June 1999.

Decker, D.T., Wise, J.O., Borer, W.S., Doherty, P.H., and Daniell, R.E., "Assessment of Ionospheric Models: Weather Specification," presented to the IUGG 99 Meeting, Birmingham, UK, July 1999 and to the URSI General Meeting, Toronto, Canada, August 1999.

Doherty, P.H., "Predicting Single-Frequency GPS Positioning Errors," seminar series presentation at the Air Force Geophysics Laboratory, August 1999.

Doherty, P.H., Decker, D.T., Sultan, P.J., Borer, W.S., and Daniell, R.E., "Assessment of Ionospheric Models: The Climatology," presented to the IUGG 99 Meeting, Birmingham, UK, July 1999 and to the URSI General Meeting, Toronto, Canada, August 1999.

Decker, D.T., Wise, J.O., Daniell, R.E., Doherty, P.H., and Borer, W.S., "Validation of an Ionospheric Specification Model," presented at the Fall AGU Meeting, San Francisco CA, December 1999.

Doherty, P.H., Decker, D.T., Sultan, P.J., Rich, F.J., Borer, W.S., and Daneill, R.E., "Comparisons Between Ionospheric Models and Observed Climatology," presented at the Fall AGU Meeting, San Francisco CA, December 1999.

Hilmer, R.V., Ginet, G.P., Kadinsky-Cole, K., Quigley, S., Decker, D.T and Doherty, P.H., "Space Environment Models Addressing Operational Hazards: An AF-GEOSPACE Perspective on Current Capabilities," presented to the 38th Aerospace Sciences Meeting of the American Institute of Aeronautics and Astronautics, Reno NV, January 2000.

Decker, D.T., Borer, W.S., Doherty, P.H., Wise, J.O., and Daniell, R.E., "Comprehensive Evaluation of Ionospheric Models," presented to the Chapman Conference on Space Weather, Clearwater FL, March 2000.

4. MEETING PROCEEDINGS

Results of our work are included in the following meeting proceedings:

Decker, D.T., Wise, J.O., Borer, W.S., Daniell, R.E., and Doherty, P.H., "Validation of PRISM: Real Time Specification," Proceedings of the 1999 Ionospheric Effects Symposium, Alexandria VA, May 1999.

Doherty, P.H., Decker, D.T., Sultan, P.J., Rich, F.J., Borer, W.S., and Daniell, R.E., "Validation of PRISM: The Climatology," Proceedings of the 1999 Ionospheric Effects Symposium, Alexandria VA, May 1999.

Smitham, M.C., Doherty, P.H., Delay, S.H., and Bishop, G.J., "Determination of Position Errors for Single-Frequency GPS Receivers," Proceedings of the 1999 Ionospheric Effects Symposium, Alexandria VA, May 1999.

Doherty, P.H., Smitham, M.C., Delay, S.H., and Bishop, G.J., "Determination of Position Errors for Single-Frequency GPS Receivers," Proceedings of the Institute of Navigation Annual Meeting, Cambridge MA, June 1999.

Hilmer, R.V., Ginet, G.P., Kadinsky-Cole, K., Quigley, S., Decker, D.T and Doherty, P.H., "Space Environment Models Addressing Operational Hazards: An AF-GEOSPACE Perspective on Current Capabilities," Proceedings of the 38th Aerospace Sciences Meeting of the American Institute of Aeronautics and Astronautics, Reno NV, January 2000.

5. JOURNAL ARTICLES

Basu, S., Groves, K.M., Quinn, J.M., Doherty, P. "A comparison of TEC fluctuations and scintillations at Ascension Island," *JASTP*, ***61***, 1219-1226, 1999. (Appendix B)

Vladimer, J.A., Jastrzebski, P., Lee, M.C., Doherty, P.H., Decker, D.T. and Anderson, D.N., "Longitude Structure of Ionospheric TEC at Low Latitude Measured by the TOPEX/Poseidon Satellite," *Radio Science*, ***Vol. 34***, #5, pp. 1239-1260, Sept-Oct 1999. (Appendix A)

APPENDIX A

Radio Science, Volume 34, Number 5, Pages 1239–1260, September–October 1999

Longitude structure of ionospheric total electron content at low latitudes measured by the TOPEX/Poseidon satellite

J. A. Vladimer, P. Jastrzebski, and M. C. Lee

Department of Electrical and Computer Engineering, Boston University, Boston, Massachusetts

P. H. Doherty and D. T. Decker

Institute for Scientific Research, Boston College, Newton, Massachusetts

D. N. Anderson

Space Vehicles Directorate, Air Force Research Laboratory, Hanscom Air Force Base, Massachusetts

Abstract. The longitude structure of ionospheric total electron content (TEC) at low latitudes has been evaluated using the NASA/Centre Nationale d'Etudes Spatiales TOPEX/Poseidon satellite. The TEC data set is given by the ionospheric range correction, which is computed from TOPEX dual-frequency altimeter measurements. The satellite's orbit allows analysis of vertically measured TEC values at approximately 30° intervals of longitude across the world at local time differences of only 6–12 min. Patterns of longitudinal dependence of the equatorial anomaly were observed during the equinoxes, summers, and winters of 1993, 1994, and 1995. TOPEX observations reveal occurrence of relative maximum anomaly TEC values in the Indian/Asian longitude sector. This dominance in TEC is seen most consistently in the Asian Southern Hemisphere. Also, a relative decrease in anomaly TEC values is evident in the western American region, which is observed primarily during equinox and winter. This configuration of the equatorial anomaly TEC is observed on a day-to-day basis at particular periods of local time. Global theoretical ionospheric model results are presented in an attempt to reproduce the distinctive longitude structure. Variability in $\mathbf{E} \times \mathbf{B}$ vertical drift velocity within specific longitude sectors is shown to be a primary factor in the longitude dependence of equatorial anomaly TEC.

1. Introduction

The forecasting of ionospheric total electron content (TEC) is of significant importance to the consistent, precise operation of ground-based and space-based systems involving radio wave signal propagation. Satellite communication, aircraft and space vehicle positioning, and surveillance systems for both defense and commercial uses require ionospheric TEC calibration. It is difficult to provide accurate predictions of TEC at low latitude due to the large spatial and temporal variations of the ionosphere in equatorial regions. Large values of TEC are observed within 30° latitude to the north and south of the magnetic equator as a result of the formation of the electromagnetic phenomenon known as the equatorial anomaly [*Appleton*, 1946]. These bilateral enhancements are formed by the perpendicular electrodynamic ($\mathbf{E} \times \mathbf{B}$) uplifting of the F region plasma in combination with the parallel plasma flow due to nonelectromagnetic forces of gravity and pressure gradients. The diurnal variation in electric field strength and ionospheric plasma density is believed to be caused by an increase in the thermospheric winds in the F region, which create ion and electron separation. Currents develop, and in response an electrostatic field is generated and interacts with the Earth's magnetic field, causing vertical plasma drifts [*Anderson*, 1981, and references therein]. Extreme day-to-day fluctuations in the equatorial anomaly have been observed, as well as variability with respect to time of day, season, longitude, solar cycle, and magnetic activity.

The NASA/Centre Nationale d'Etudes Spatiales (CNES) TOPEX/Poseidon satellite provides worldwide over-ocean values of vertical TEC within a longitude range of 0°–360° and a latitude range of

Paper number 1999RS900060
0048-6604/99/1999RS900060$11.00

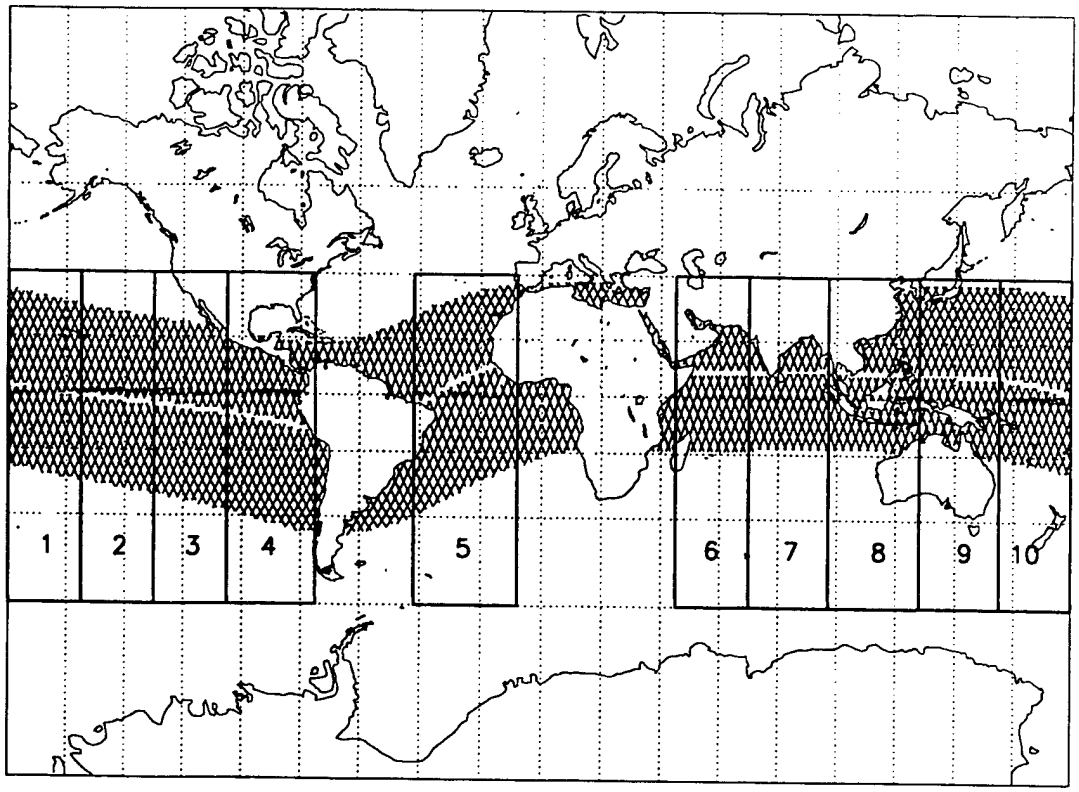

Figure 1. TOPEX coverage at low magnetic latitude is shown. Each of 10 defined bins contains the data from the same 10 days and local times.

−66°–66°. In this study the TOPEX data set was utilized to evaluate the low-latitude longitudinal structure of the ionosphere in terms of average values of TEC and repeated patterns of behavior of the equatorial anomaly. Ionospheric model simulations were generated in an attempt to reproduce the observed consistent configurations of TEC within specific longitude sectors. Models employed were the Air Force Research Laboratory parameterized ionospheric model (PIM) and the global theoretical ion-

Table 1. Descriptions of Bins in Terms of Longitude, Latitude, and Declination Range at the Magnetic Equator

Longitude Sector	TOPEX Bin	Geographic Longitude Range (Magnetic Equator Crossing)	Geographic Latitude Range	Declination Range
Pacific	1	180°E–206°E	+1 to −1	11°E–12°E
	2	206°E–232°E	−1 to −5	10°E–12°E
American	3	232°E–255°E	−5 to −9	6°E–10°E
	4	255°E–285°E	−9 to −14	1°E–6°E
Brazilian	5	318°E–352°E	+4 to +11	8°W–10°W
Indian/Asian	6	45°E–70°E	+8 to +9	8°W–10°W
	7	70°E–97°E	+8 to +10	2°W–8°W
	8	97°E–128°E	+8 to +10	2°W–3°E
	9	128°E–155°E	+7 to +8	3°E–8°E
Pacific	10	155°E–180°E	+1 to +7	8°E–11°E

Bins are described in terms of longitude sector. The ranges of geographic longitude, geographic latitude and declination are referenced to the magnetic equator.

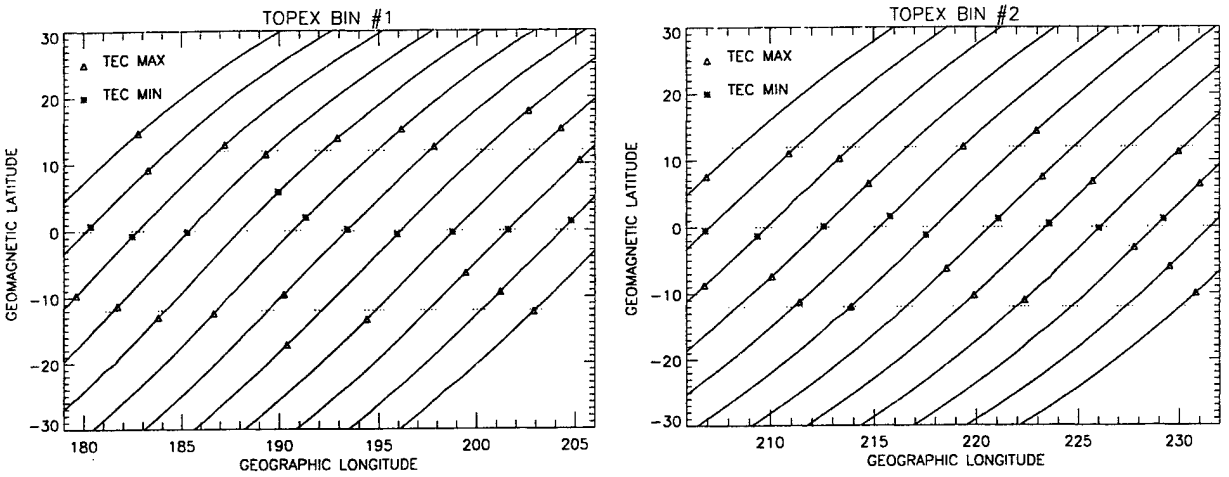

Figure 2a. TOPEX passes within adjacent bins 1 and 2 are shown. Equatorial anomaly crest and trough values are represented by triangles and stars, respectively.

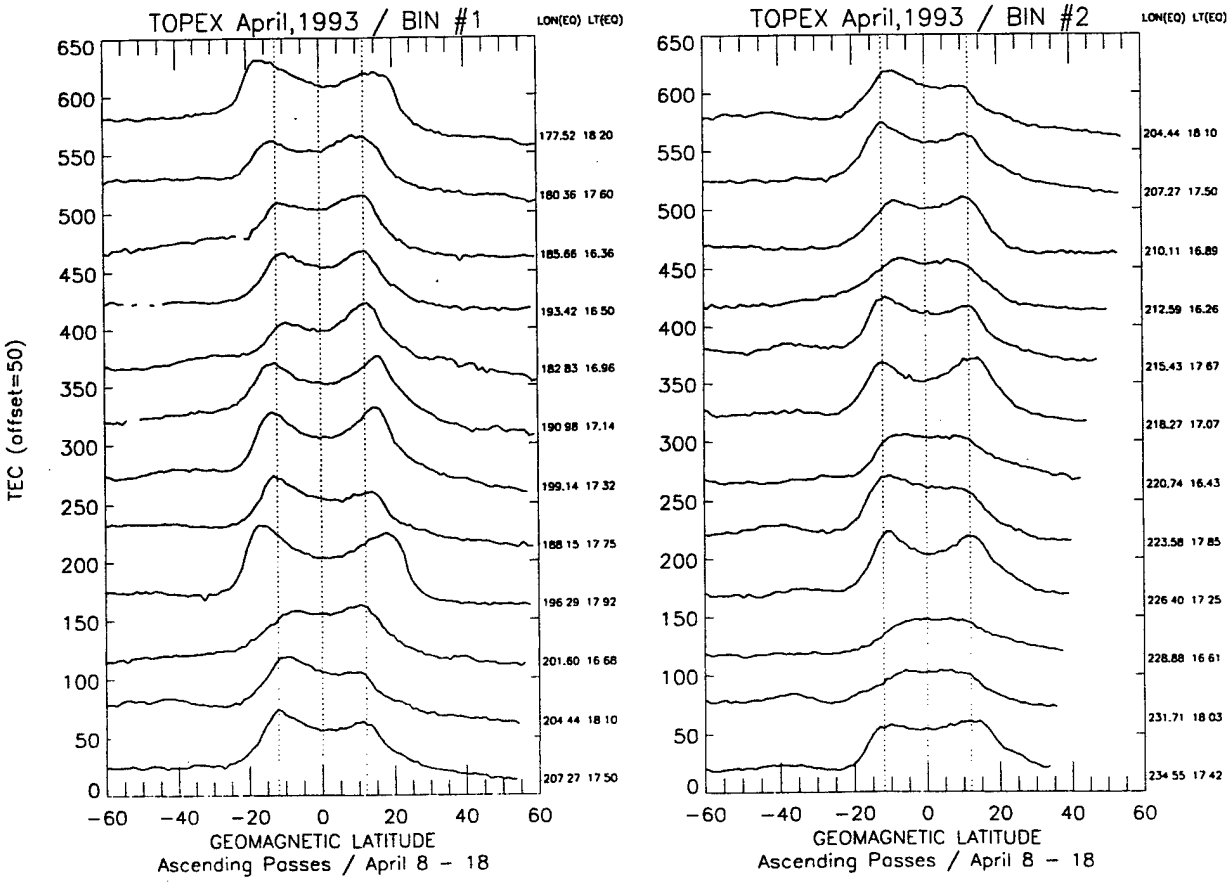

Figure 2b. Data from bins 1 and 2 illustrate the differences between anomaly shape and variability within bins of close proximity.

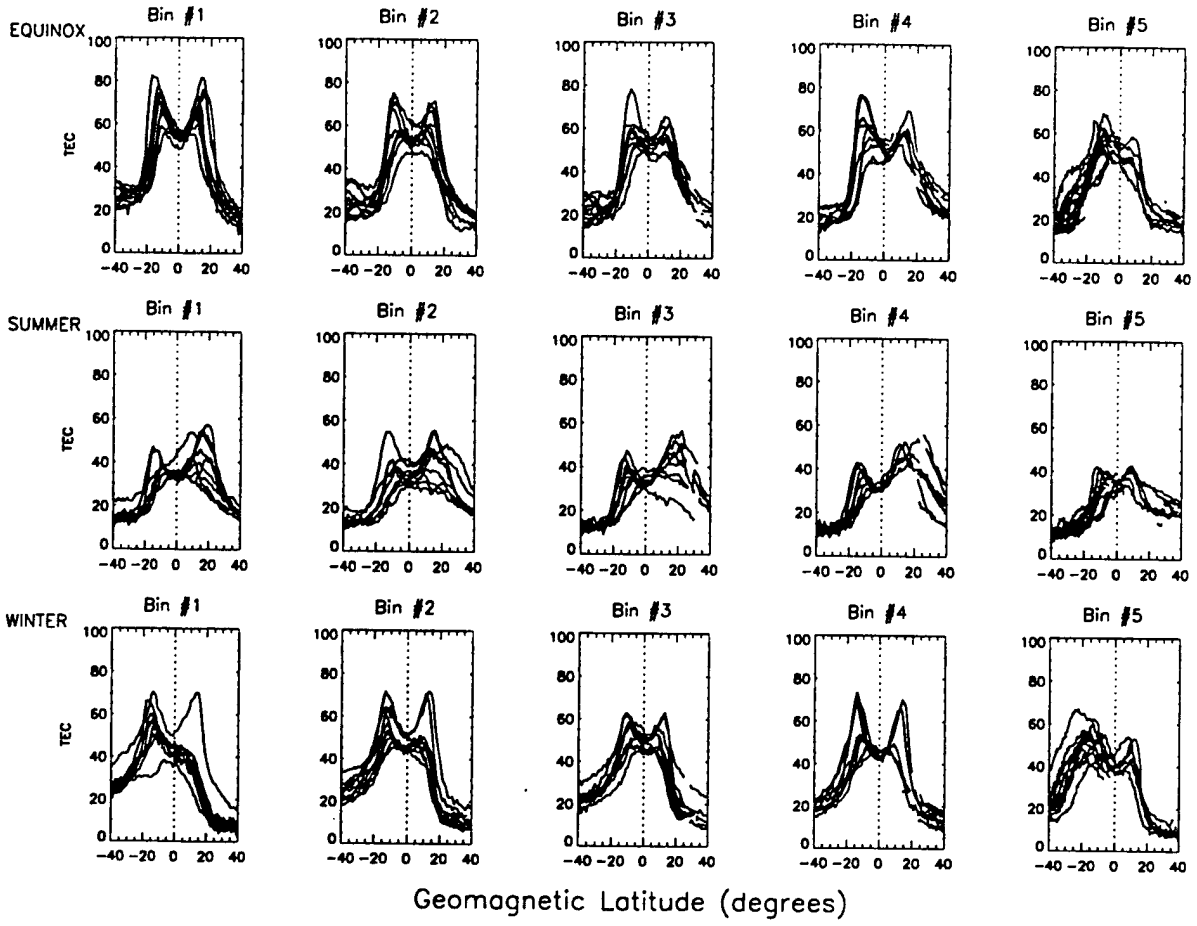

Figure 3a. Scatterplots from bins 1–5 show data during spring equinox, summer, and winter of 1993.

ospheric model (GTIM). These theoretical models were chosen for their ability to test the sensitivity of the ionosphere to variations in inputs such as $\mathbf{E} \times \mathbf{B}$ vertical drift velocity, ion and electron temperatures, and other specific geophysical conditions which are described in section 3. The TOPEX coverage at equatorial anomaly latitudes and the defined longitude bins used for this work are shown in Figure 1. Table 1 describes each bin in terms of the longitude, latitude, and declination range at the magnetic equator. Specifically, the range of geographic longitude is given by the TOPEX pass crossings at the geomagnetic equator. The geographic latitude extent of the magnetic equator is indicative of the difference between the geographic and geomagnetic equators. Finally, the range of values and direction of declination at the magnetic equator within each bin are listed.

Previous studies have revealed discrepancies in TEC values within various longitude sectors using data collected at low-latitude ground stations [*Walker*, 1981; *Su et al.*, 1995]. Probable reasons for the longitudinal variability at these specific latitudes have been presented. Contributing factors include (1) the geomagnetic equator not being parallel to the geographic equator, (2) variations in magnetic declination, and (3) variations in electric and magnetic fields. The variability in range of the Earth's magnetic field over the magnetic dip equator has been described as the cause of the variation of equatorial ionospheric conductivity with longitude [*Rastogi*, 1962]. The resulting $\mathbf{E} \times \mathbf{B}$ vertical drift and neutral wind velocities are described as the primary drivers that dictate the movement of ionization and directly influence the development of the equatorial anomaly. More recent studies have used TOPEX data to evaluate specific

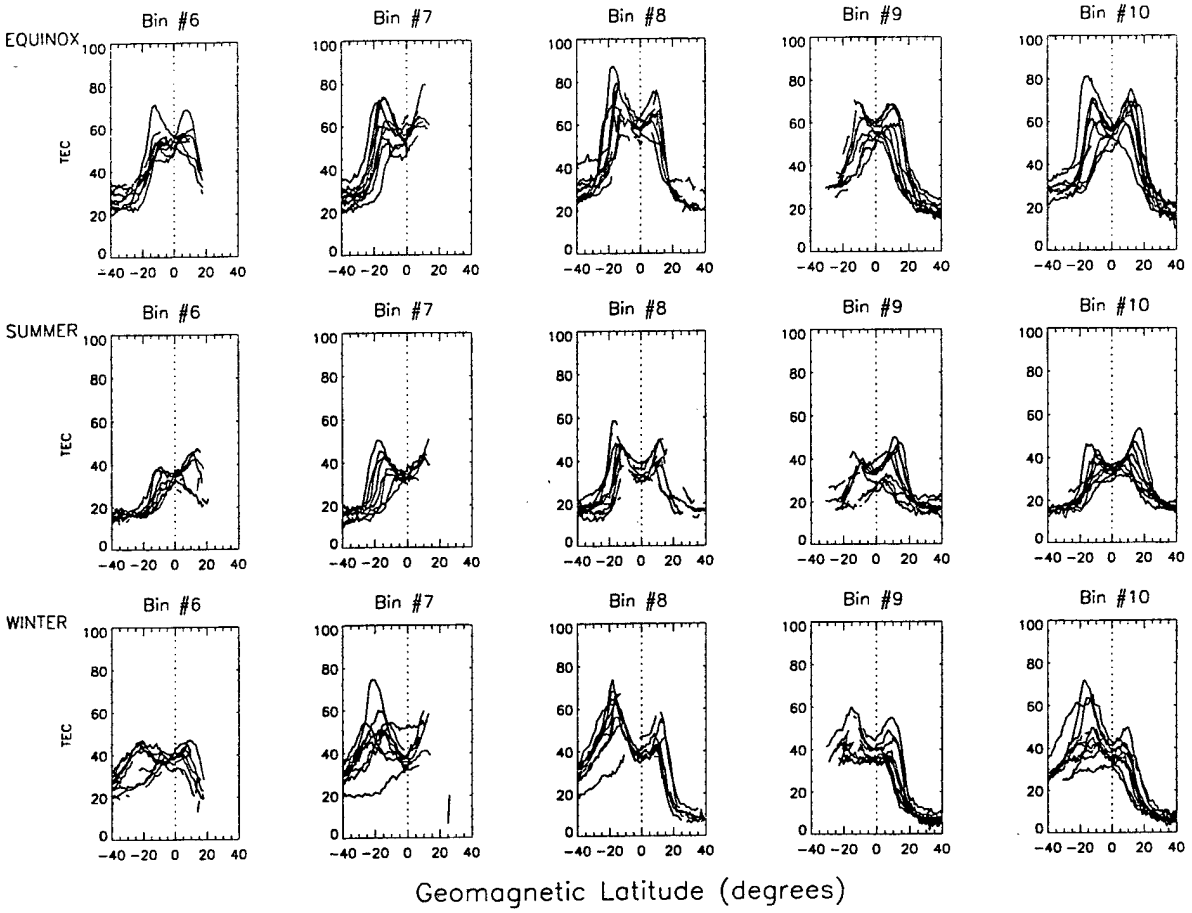

Figure 3b. Scatterplots from bins 6–10 show data during spring equinox, summer, and winter of 1993.

events and longitude structure during a particular seasonal period [*Forbes et al.*, 1997]. Additional works compare TOPEX to the International Reference Ionosphere (IRI) model results, with emphasis on interhemispheric asymmetry of the equatorial anomaly [*Bilitza et al.*, 1996]. The present study evaluates low-latitude TOPEX data during the periods of equinox, summer, and winter of 1993, 1994, and 1995. The seasonal focus of the model simulations is spring equinox 1993 at solar moderate conditions and relatively low magnetic activity ($Kp \leq 4$). Simple modifications made to the vertical drift inputs of the GTIM provide low-latitude TEC values that approximate the TOPEX time-averaged longitude configuration. In section 2 the TOPEX orbit and dual-frequency altimeter measurements are reviewed, followed by a discussion of the limitations in the application of the TOPEX data to ionospheric research. Model calculations of TEC values and the comparison with the TOPEX data are presented in section 3. Discussion is given in section 4, and finally, conclusions are drawn in section 5.

2. Measurements and Observations

2.1. TOPEX TEC Measurements

The TOPEX/Poseidon satellite was launched in 1992 for the study of global ocean dynamics. The satellite has an orbital altitude of 1336 km (equatorial reference) and an inclination of 66°. One full revolution, which is achieved in 112 min, consists of two passes: An ascending pass spans −66° to 66° latitude; a descending pass spans 66° to −66° latitude. Consecutive revolutions are offset to the west by approximately 30°. This TOPEX coverage provides the ability to observe TEC variability across the world in 1 day at

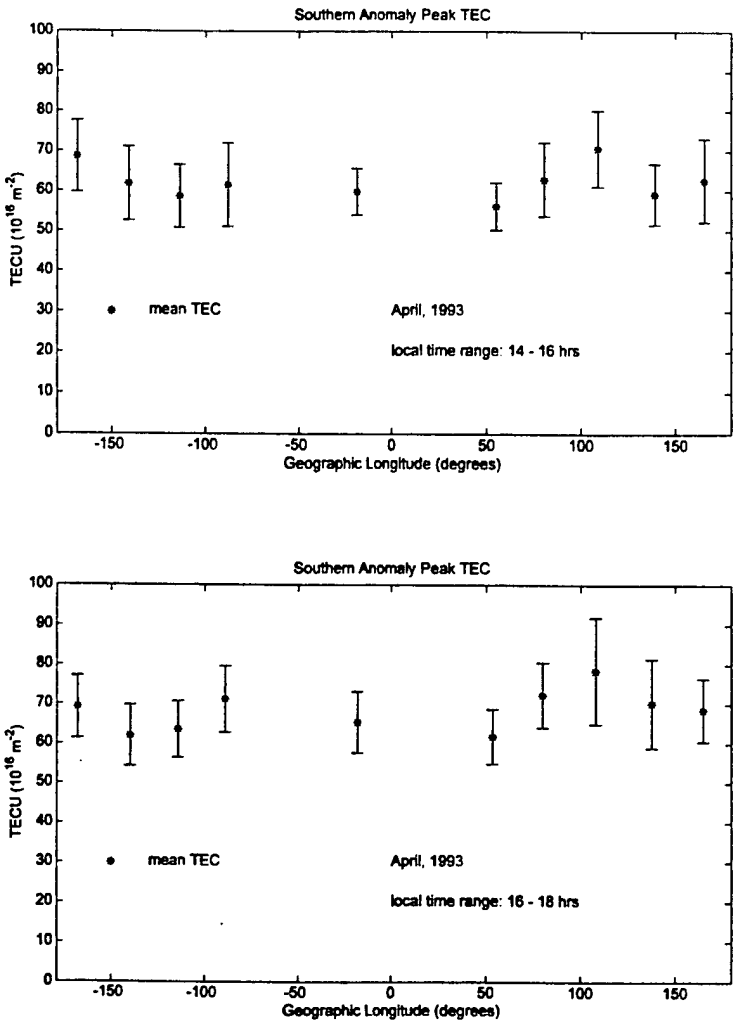

Figure 3c. Standard deviations are plotted with the mean total electron content (TEC) of the southern anomaly peaks. The bottom plot corresponds to Figures 3a and 3b (1600–1800 LT, April 1993). The top plot represents data from 1400–1600 LT.

30° intervals at approximately the same local time. There are 127 revolutions (254 passes) in a TOPEX cycle, which covers the same surface tracks every 10 days. The differential between UT and LT, in combination with the "overlap" required to accomplish ice-free ocean coverage, results in a 2-hour loss of local time for each consecutive 10 days of universal time.

TOPEX orbital speed is 7.2 km s^{-1}, and altimeter measurements are obtained at a rate of one per second. The ionospheric correction and vertical TEC are computed from TOPEX dual-frequency range measurements (5.3 GHz, C band, and 13.6 GHz, Ku band). The measured range is give by

$$R_{\text{measured}} = R_{\text{true}} + \Delta R_{\text{ionosphere}} + \Delta R_{\text{other}} \quad (1)$$

where R_{true} is the true range, $\Delta R_{\text{ionosphere}}$ is the ionospheric range error at the frequency, C or Ku and ΔR_{other} are the range errors due to other frequency-dependent and non-frequency-dependent sources. The range error, $\Delta R_{\text{ionosphere}}$ (centimeters), has the form b_C/f_C^2 or b_{Ku}/f_{Ku}^2, where b_i equals 40.3 $\text{TEC}_{\text{vertical}}$, with f_i expressed in gigahertz. The measured range

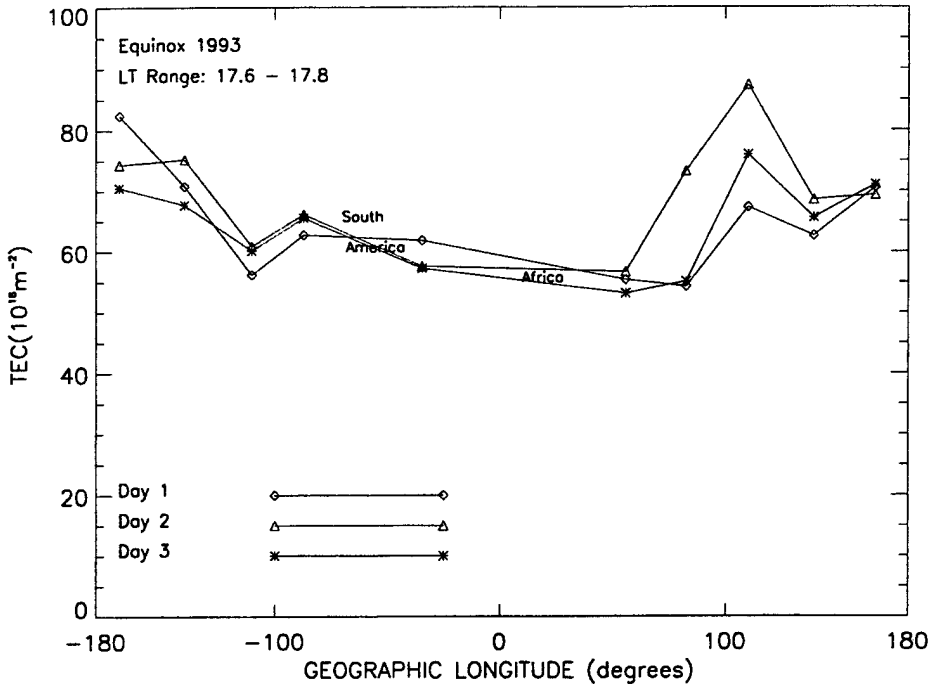

Figure 4. Data from 3 days at approximately the same local time are represented from each bin. Southern anomaly TEC values reveal a repeated longitude configuration.

equations for C and Ku bands provide an expression for the differential ionospheric correction:

$$\Delta R_{\text{ionosphere}} = [40.3\text{TEC}_{\text{vertical}}][(f_{\text{Ku}}^2 - f_{\text{C}}^2)/f_{\text{C}}^2 f_{\text{Ku}}^2] \quad (2)$$

The vertical TEC follows as

$$\text{TEC}_{\text{vertical}} = \Delta R_{\text{ionosphere}}[f_{\text{C}}^2 f_{\text{Ku}}^2/(f_{\text{Ku}}^2 - f_{\text{C}}^2)40.3] \quad (3)$$

One TEC unit (TECU) (10^{16} el m^{-2}) corresponds to 12.17-mm range error at the given TOPEX altimeter frequencies. The uncertainty in the TOPEX ionospheric correction has been estimated to be approximately 0.5 cm, which corresponds to 0.41 TECU [*Imel*, 1994].

TOPEX satellite data present limitations in applications to studies involving TEC. Several constraining factors are described as follows:

1. The instruments do not obtain readings over land, resulting in discontinuities in the data set.

2. Because of the 66° inclination of the orbit, careful analysis of data from individual satellite passes is required. Differences in longitude (local time) exist between altimeter measurements of the two crests of the equatorial anomaly. The variations in longitude (local time) can range from 10°− to 15°+ (40− min to 60+ min) depending on the latitudinal extent of the anomaly.

3. NASA TOPEX and CNES Poseidon share an antenna, which causes 10-day interruptions of the data set.

4. The use of data from a transiting satellite does not allow separation of diurnal from seasonal variability in TEC. For instance, equinox (March, April or September, October) represents 12 hours of local time, while summer (May–August) or winter (November–February) represents 24 hours of local time.

Observations are presented in the next section. Data comparisons which are extended across the 10 bins reveal a trend that is maintained over local time and season.

2.2. TOPEX TEC Observations

An example of TOPEX data from April 1993 is shown in Figures 2a and 2b. The data were processed by averaging over 1° of satellite orbit. (One degree corresponds to approximately 16 s of flight and 110 km of ground track.) Figure 2a shows a closer look at bins 1 and 2 in which 30° × 30° north and south subbins are created and averaged separately to compensate for the inclination of the orbit. The first two

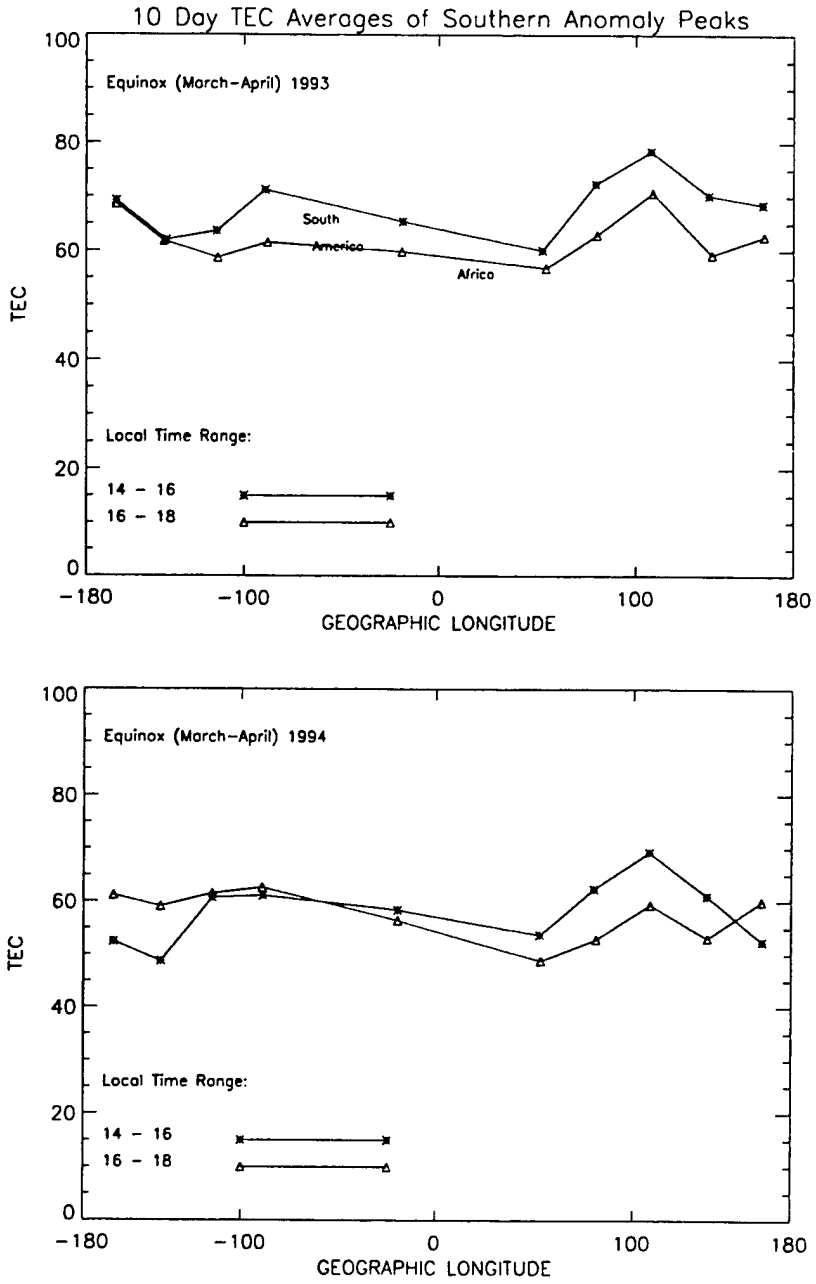

Figure 5. The longitude pattern is evident in the seasons of spring equinox, summer, and winter of 1993, 1994, and 1995.

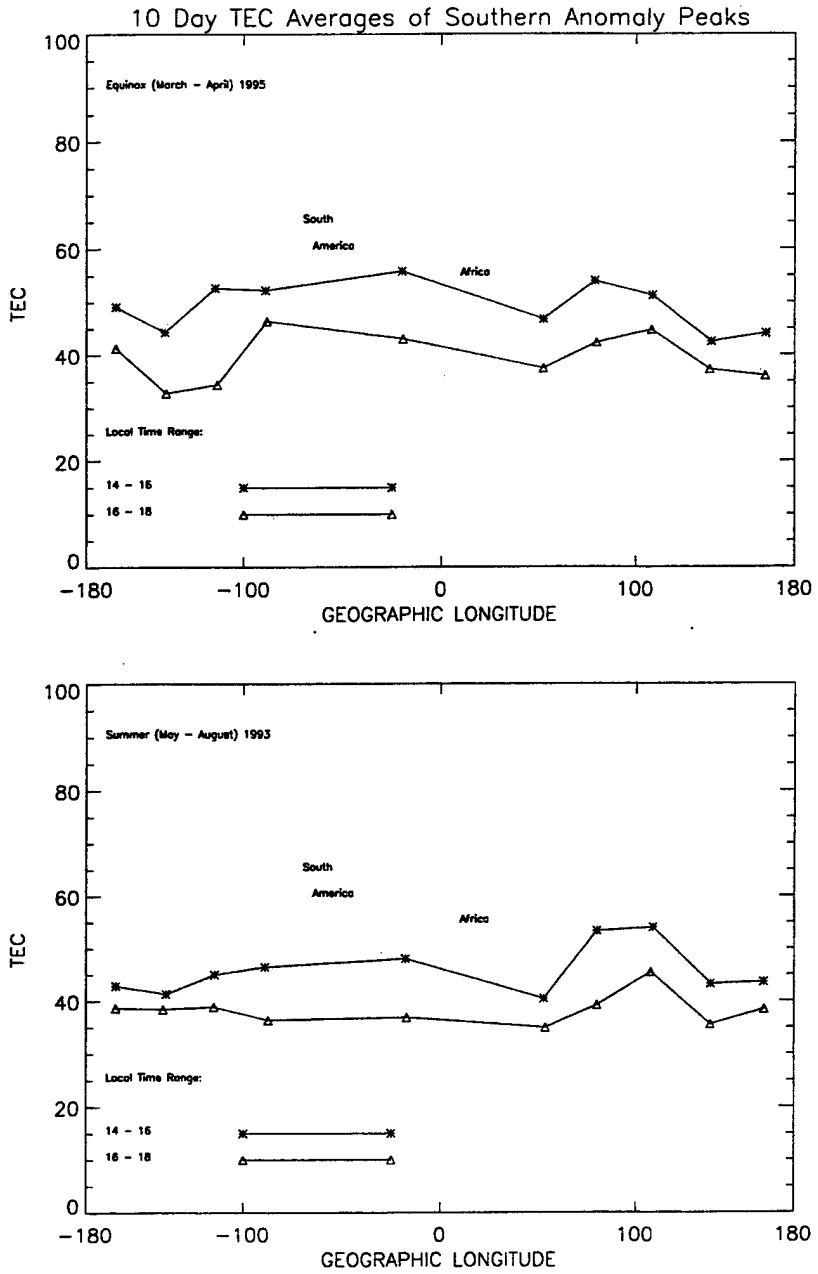

Figure 5. (continued)

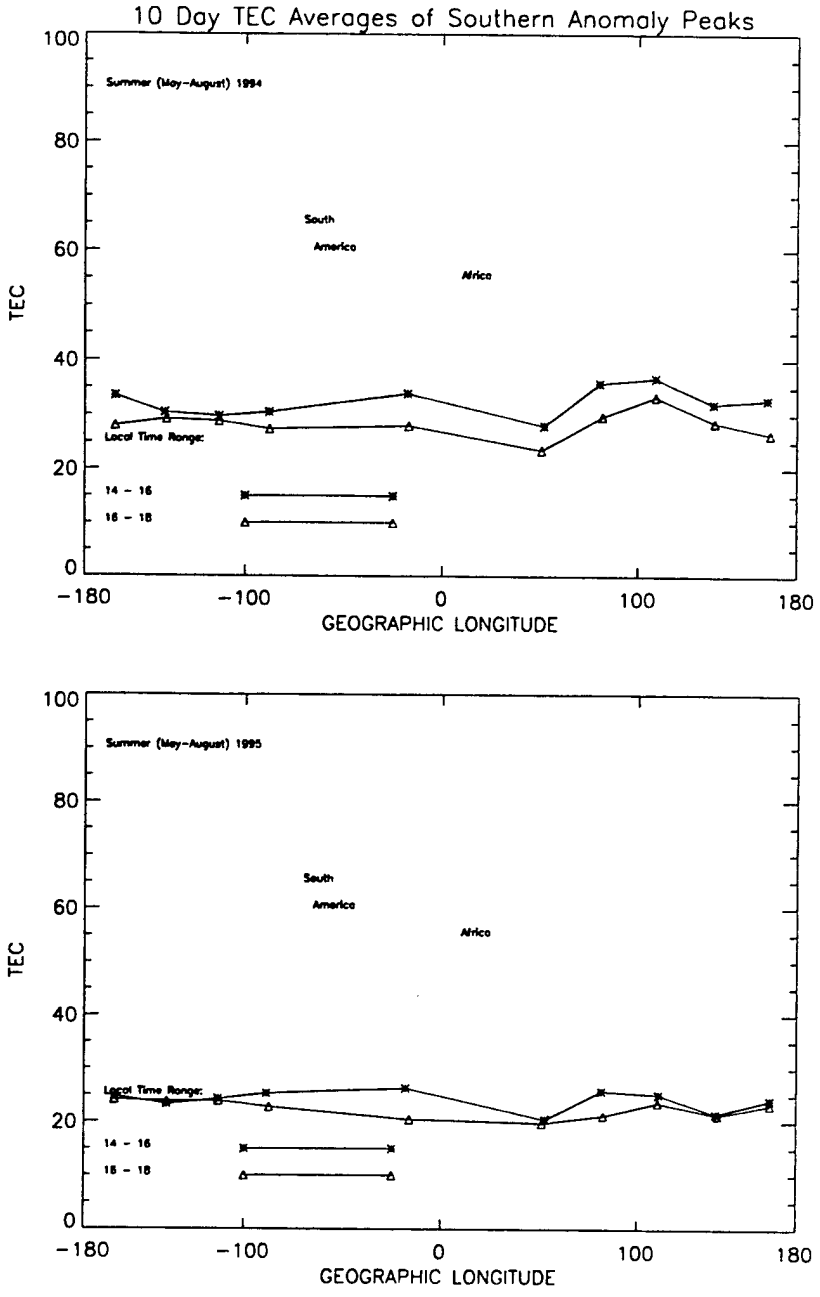

Figure 5. (continued)

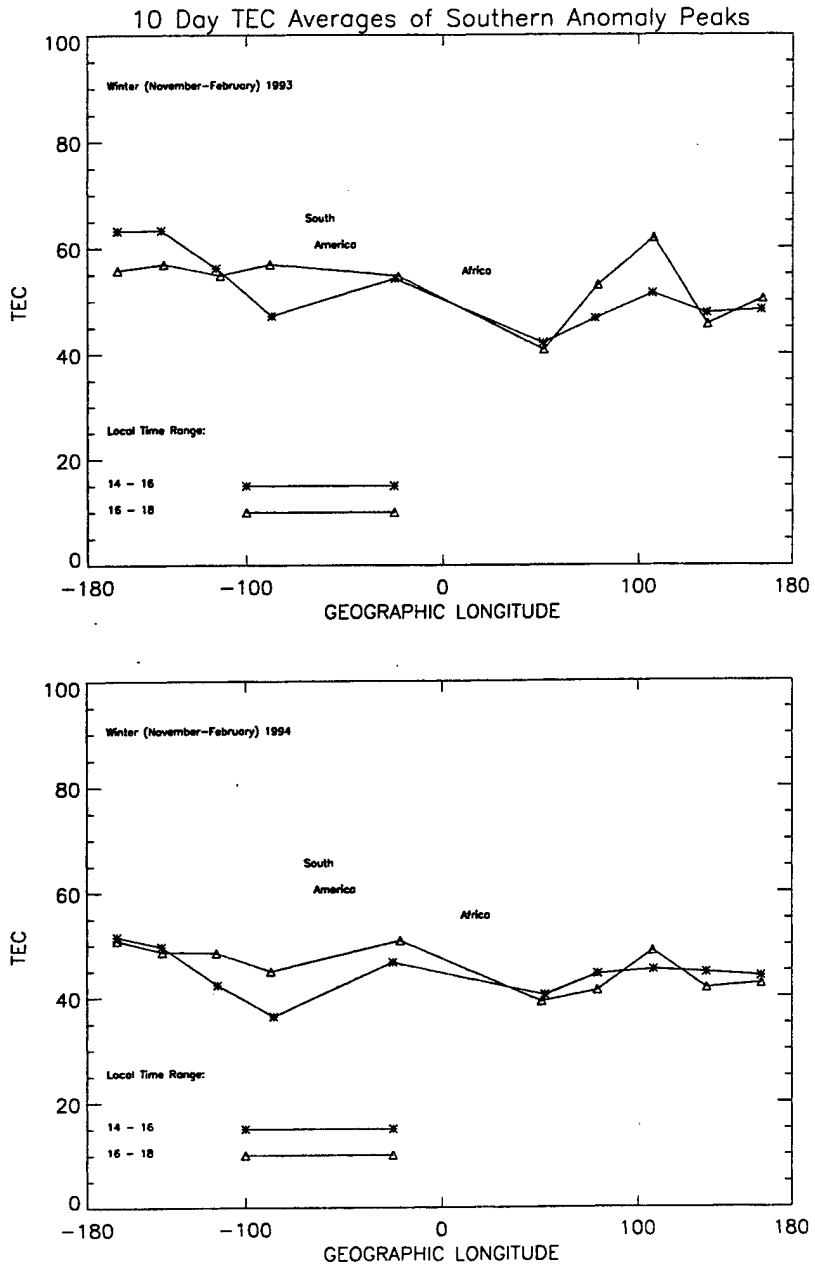

Figure 5. (continued)

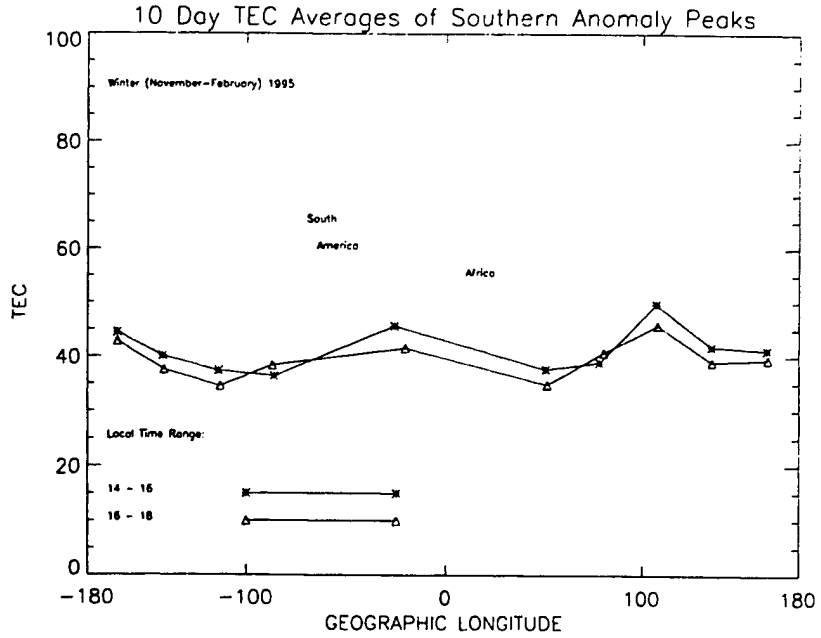

Figure 5. (continued)

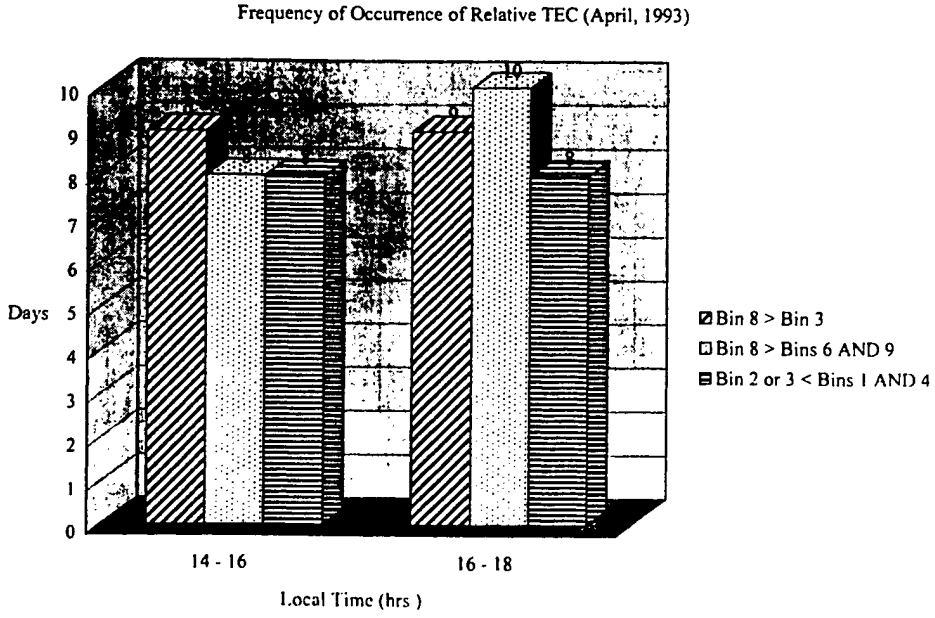

Figure 6. Each bar shows the number of days that one longitude bin's TEC value (southern anomaly peak) is greater or less than that of another bin. This consistent relative TEC pattern is representative of the TOPEX average longitude configuration.

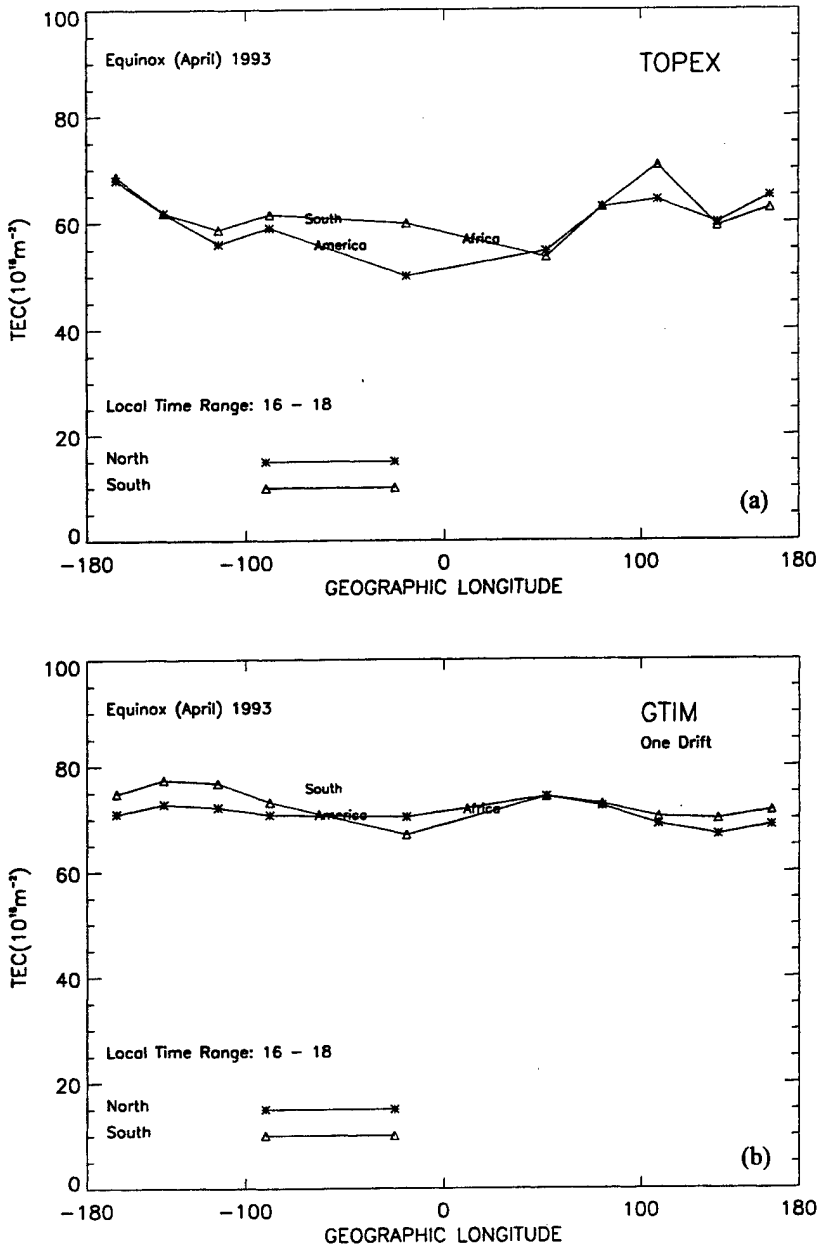

Figure 7. TOPEX averages of north and south anomaly peaks during spring equinox at local times between 1600 and 1800 (Figure 7a) are compared with model results from the global theoretical ionospheric model (GTIM) with one drift input (Figure 7b) and GTIM with four drift inputs (Figure 7c).

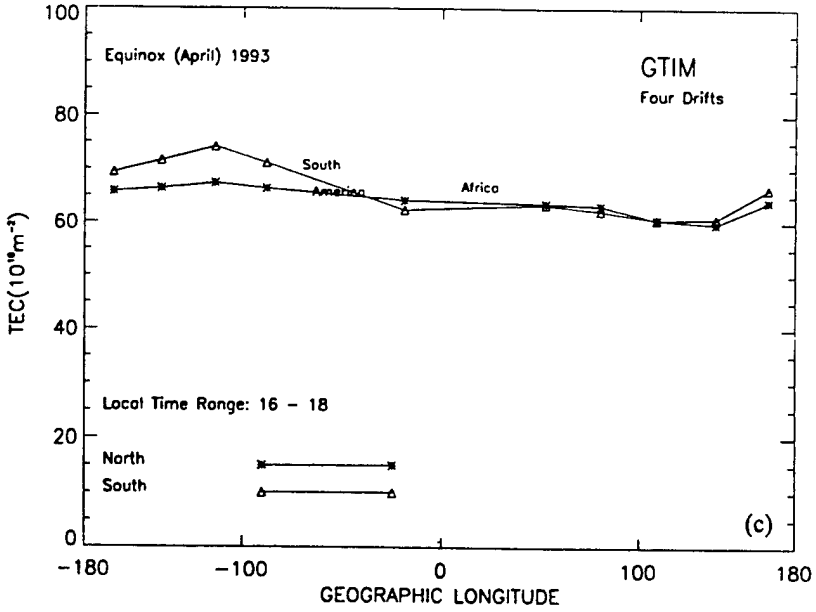

Figure 7. (continued)

passes and the last two passes are same-day passes and are shared with adjacent bins, thereby separating the TEC data (north from south) at bin boundaries. The maximum and minimum points of the equatorial anomaly are indicated symbolically. Lines are drawn at $\pm 12°$ magnetic latitude to accentuate the difference in latitudinal extent of the anomaly in the adjacent bins 1 and 2. This feature is also evident in Figure 2b, where the passes within each bin are plotted. Other characteristics to be observed are crest-to-trough ratios, hemisphere differences, and TEC gradients. Stronger anomaly formation with higher TEC values, larger gradients, and crest-to-trough ratios are seen in bin 1 compared with bin 2. Hemisphere differences are not significant or consistent in either bin.

Figures 3a and 3b illustrate the variability in TEC during spring equinox (April), summer (August), and winter (December) at 1600–1800 LT within bins 1–5 and bins 6–10, respectively. Several features of the equatorial anomaly can be examined in these scatterplots. (A compromise in the data occurs in the Northern Hemisphere in bins 6 and 7 due to the presence of landmass.) Common to most longitude bins is the noticeable hemisphere asymmetry in summer and winter. Higher, more variable TEC is observed in the Northern Hemisphere in summer (reference to Northern Hemisphere summer and winter) and in the Southern Hemisphere in winter, while the equinox period reveals more symmetric anomaly values. The hemisphere aymmetry in TEC is most likely due to changes in strength and direction of neutral wind. A trend of dominant TEC is seen in the Asian Southern Hemisphere (bin 8) during all seasons (see Figure 3b). In addition, a relative decrease in TEC is noticeable in bins 2–3, which is most evident in equinox and winter due to the larger Pacific TEC values observed during these seasons (see Figure 3a).

This longitude trend can be highlighted by focusing on peak TEC measurements within each bin. Data results shown in Figures 3c, 4, and 5 are concentrated in the south where there is the least land interruption of the TEC values. Both plots in Figure 3c show standard deviations of mean peak TEC values (southern anomaly crest) within the 10 longitude bins over two consecutive 10-day periods in April 1993. The bottom plot corresponds to the spring equinox data of Figures 3a and 3b for 1600–1800 LT. The top plot corresponds to April data for 1400–1600 LT. In spite of the expected variability in absolute TEC values, a distinct mean longitude pattern exists. Figure 4 shows TEC peak values of the southern anomaly crest on each of three consecutive days. The longitude pattern clearly is repeated on a day-to-day basis. Figure 6 illustrates the frequency of occurrence of the relative maximum TEC in the Indian/Asian region and the

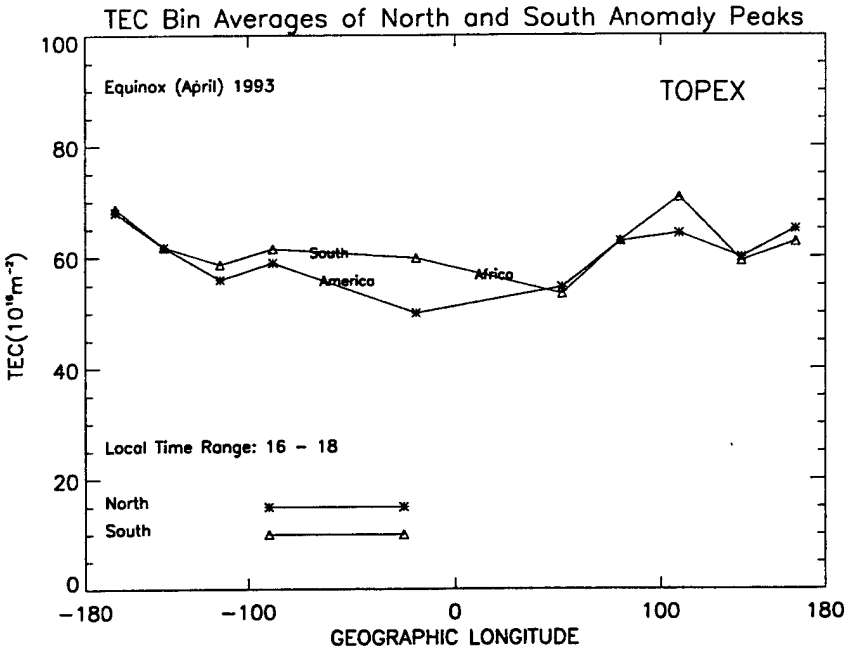

Figure 8a. TOPEX averages from Figure 7 are repeated for model comparison.

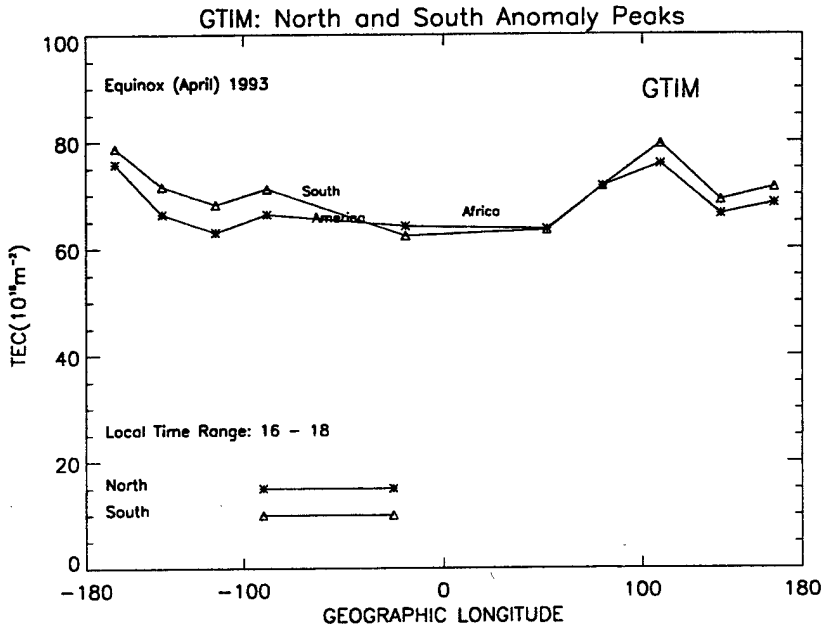

Figure 8b. GTIM results after drift weighting factor manipulation show a longitude pattern similar to TOPEX data.

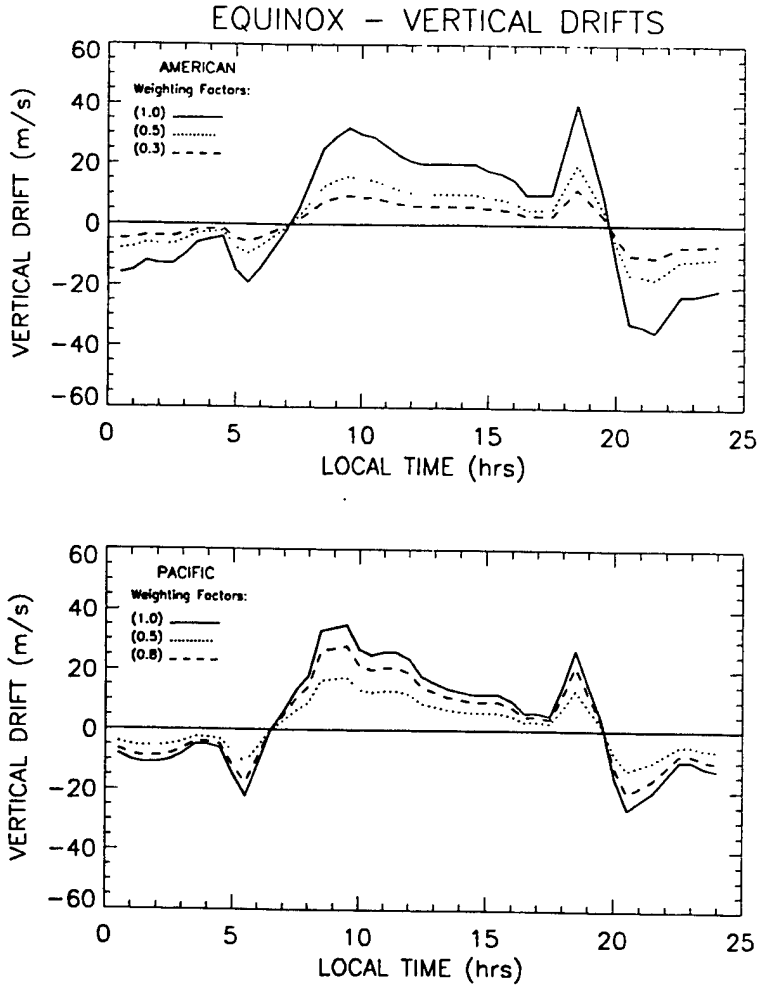

Figure 9. The four empirical drifts from *Fejer et al.* [1995] are shown (solid lines). Half-weighting was required to acquire TEC values comparable to the parameterized ionospheric model (PIM) (dotted lines). Variable weighting achieves results closer to the TOPEX configuration (dashed lines).

relative diminishment of TEC in the western American region for the April periods. Each bar in the plot represents the number of days that one region's peak southern TEC value is greater or less than that of another region. Describing the plot from left to right, the first bar represents bin 8 greater than bin 3; the second bar represents bin 8 greater than both bins 6 and 9; and the third bar represents bin 2 or 3 less than both bins 1 and 4. Results are shown for time ranges of 1400–1600 and 1600–1800 LT. Figure 5 illustrates the longitude behavior of 10-day averaged maximum TEC values of the southern anomaly crest within 10 bins. The configuration of longitude dependence is maintained over a 4- to 6-hour local time range. The analysis is shown for spring equinoxes, summers, and winters of 1993, 1994, and 1995. The data from 1400–1600 and 1600–1800 LT are shown separately to illustrate that although TEC values change, the overall configuration is similar during both time ranges. The most consistent occurrence of this pattern of TEC is seen during 1400–1800 LT and is altered when earlier and later local times are evaluated. The existence of a relative maximum in bins 7 and 8 and a relative minimum in bins 2 and 3 is evident to a certain extent in all seasons. The feature of stronger Indian/Asian peak values is seen consistently, although it diminishes with later local times and decreasing solar cycle. These results are in agreement with previous studies [*Su et al.*, 1995] which have evaluated summer data from stations near East Asia

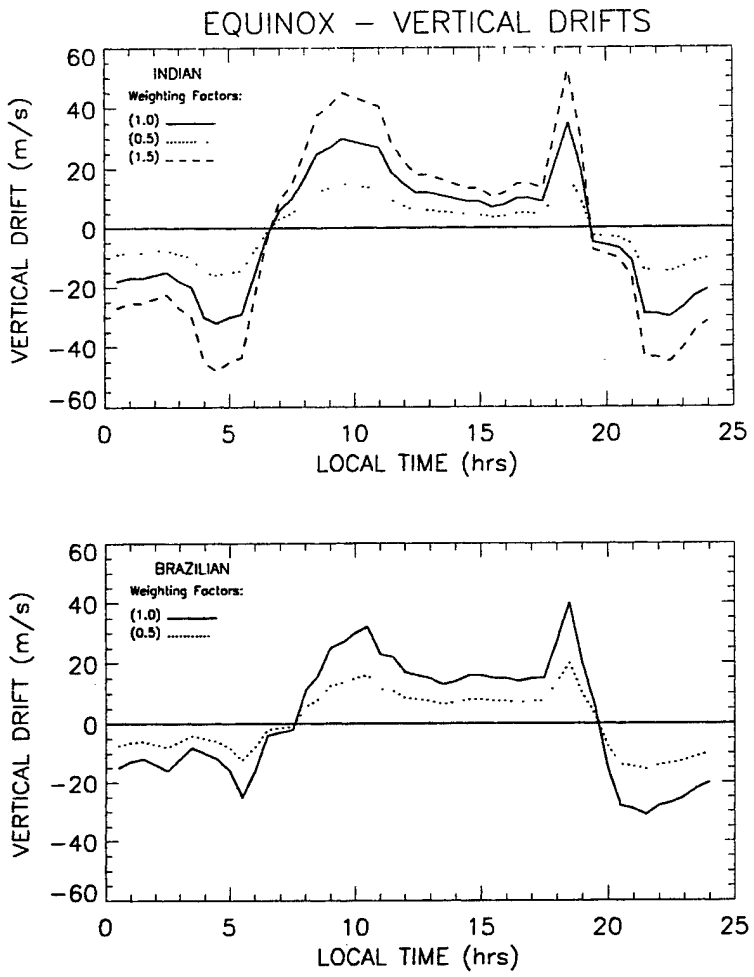

Figure 9. (continued)

and mid-Pacific longitudes. The enhanced TEC values in the Indian region are also consistent with previous findings of a maximum in the strength of the electric field over the magnetic equator in India during the equinox period [*Rastogi*, 1993]. In addition, *Rastogi* [1962] has described the intensity of the magnetic field (H) as strongest in the Indian region and at a minimum in South America, while the range of H is greatest in the American region and least in India. The relative minimum trend in the western American/Pacific bins 2 and 3 is most obvious in equinox and, to a lesser extent, in summer due to decreasing TEC in bins 1 and 4. Also, in winter the relative minimum appears to shift toward bins 3 and 4, while bins 1 and 2 are maintained at values comparable to bin 8 in the Indian/Asian region.

3. Results of Model Calculations

The global theoretical ionospheric model (GTIM) is designed to generate the ionospheric conditions based on several parameters given for a specific day. This model uses ion continuity and momentum equations to calculate electron density profiles (EDPs) and total electron content (TEC) for a particular longitude and day of the year. Specifically, for the F region, the time-dependent ion (0^+) continuity equation is utilized. The component parallel to the electric field velocity is derived from electron and ion equations; the perpendicular component is the $\mathbf{E} \times \mathbf{B}$ drift. In addition to the electric field, the input parameters for the model include the neutral constituents, temperature, and winds. The ion and electron tempera-

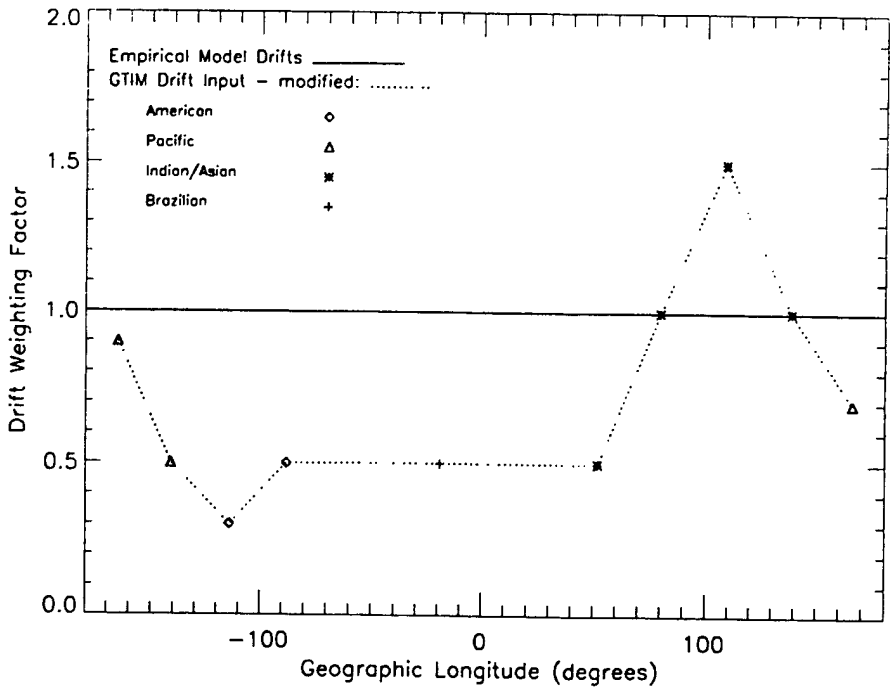

Figure 10. Longitude sector vertical drifts and weighting factors are indicated for each of the 10 TOPEX bins. Required modification of weighting factors is shown. These factors were used for drift inputs to GTIM, giving results that approach TOPEX observations.

tures, solar EUV fluxes, and values of the magnetic field are also utilized [*Decker et al.*, 1997]. The parameterized ionospheric model (PIM) is a computationally efficient ionospheric and plasmaspheric model developed by the Air Force Research Laboratory to aid a global parameterized real-time ionospheric specification model (PRISM). The ionospheric part of the model consists of a database of results of several regional theoretical ionospheric models and a FORTRAN code designed to extract this data for particular geophysical conditions and spatial coordinates. While the ionospheric part of the model is based solely on theoretical climatology, the plasmaspheric portion of PIM is based on the Gallagher plasmaspheric (H^+) empirical model. The geophysical parameters required are date and time, magnetic activity index (K_p), orientation of the interplanetary magnetic field, solar activity indices ($F_{10.7}$), and sunspot number (SSN). The model calculates the EDPs and TEC between the altitude of 90 and 25,000 km [*Daniell et al.*, 1995].

The results shown in Figure 7 are focused on 1993 spring TEC data. Averages of both the south and north maximum TEC values (i.e., the anomaly crests) are presented for 1600–1800 LT. TOPEX (Figure 7a) shows hemisphere differences, which are most noticeable in bins 5 and 8, with small asymmetries in bins 3, 4, and 10. GTIM was run at approximately the average bin longitudes, first utilizing one drift input (Figure 7b) for all 10 longitude regions and then using four vertical drift inputs (Figure 7c). These average drifts were developed from AE-E satellite data which were collected at moderate to high solar flux conditions [*Fejer et al.*, 1995]. The weighting factor for these four longitude sector drifts was decreased by 0.5 in order to obtain GTIM results that were comparable to TOPEX TEC values, but longitude features were not reproduced. Most remarkable is the lack of TEC enhancement in the Pacific bin 1 and in the Indian/Asian bins 7 and 8. Overall, TEC values are higher than TOPEX, with indications of hemisphere asymmetry primarily in the Pacific and American sectors. PIM results (not shown) demonstrate a longitude pattern similar to GTIM, with a slight decrease in TEC and minimal hemisphere asymmetry. There is an insignificant difference in the GTIM outputs resulting from the use of one drift or four drifts. This outcome is expected due to the lack of longitude

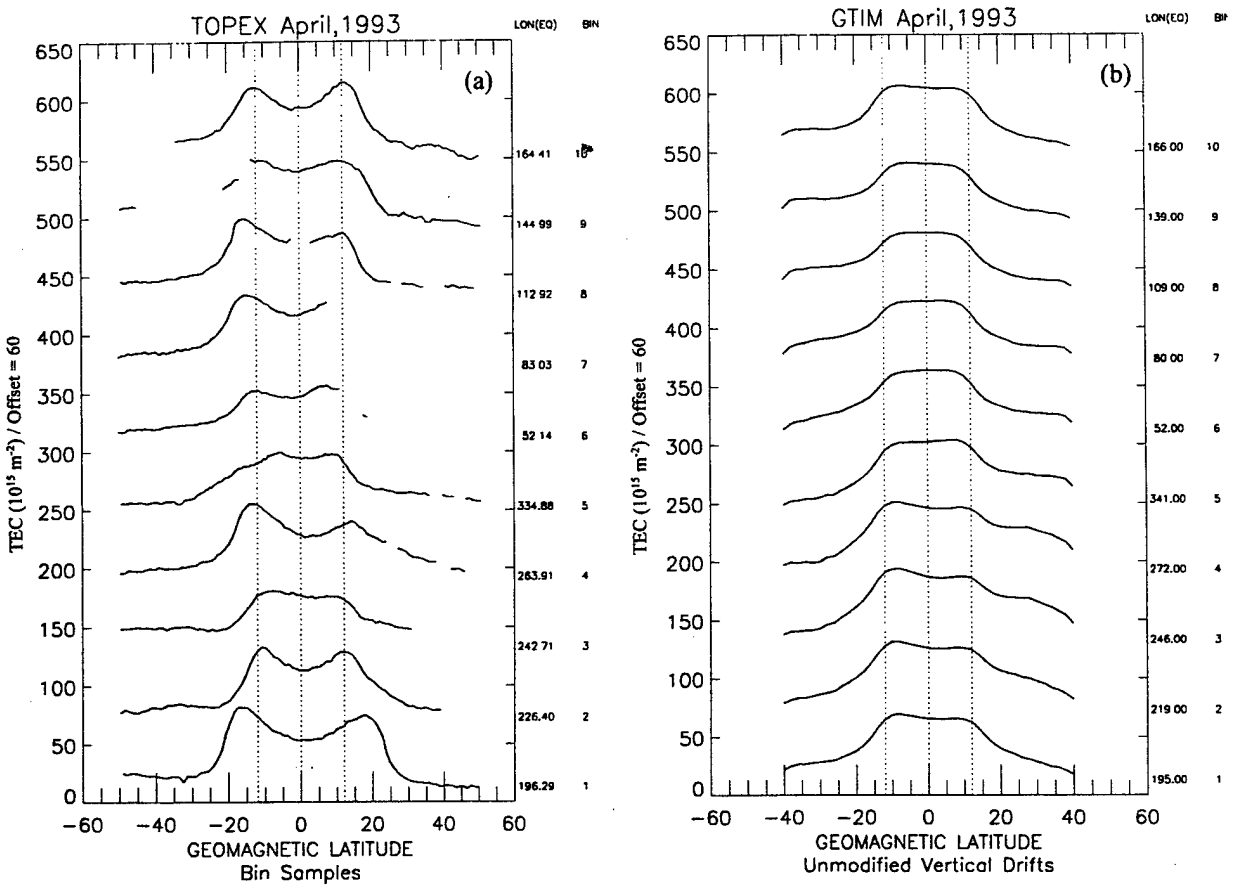

Figure 11. (a) TOPEX bin samples taken at approximately the average bin longitudes at 1630–1730 LT are shown. (b) GTIM results are shown from runs made at average bin longitudes. (Drift inputs are at half-weighting.) TOPEX longitude dependence is not observed. (c) GTIM results are shown from runs made at average bin longitudes. (Drift inputs are at variable weighting.) TOPEX peak TEC values are approximated.

dependence in the four empirical model average drifts during the equinox period.

Drifts were then altered again by a simple scaling manipulation which allowed GTIM to reproduce the TOPEX longitude shaping. Figures 8a and 8b illustrate the TOPEX and GTIM results, respectively. The TEC values are higher than TOPEX by 5–10 TECU, and hemisphere asymmetries are similar, with the exception of bins 5 and 10, which are reversed. The vertical drifts that have been modeled for four longitude sectors are shown in Figure 9. The solid lines represent the average drifts given by *Fejer et al.* [1995]. The dotted lines indicate the half-weighting that brought the GTIM results closer to the TOPEX values. The dashed lines are the input drifts that reproduced the TOPEX configuration. These manipulated drifts appear to be within the scatter representation of the drift measurements [*Fejer et al.*, 1995]. Figure 10 indicates which of the four modeled drifts were used for the 10 longitude bins and the required changes in the drift weighting factors. Finally, Figure 11 shows specific anomaly shapes within bins 1–10. (Bin numbers are indicated to the right of the plots.) On the far left (Figure 11a), TOPEX passes chosen from each bin (at the GTIM run longitudes) are compared with the GTIM results with unmodified drifts (Figure 11b) and to the GTIM results with modified drifts (Figure 11c). The increase in drifts for the Indian/Asian and Pacific sectors caused not only higher TEC values but also an increase in the latitude spread of the crests and larger crest-to-trough ratios. A decrease in the drifts in the western American

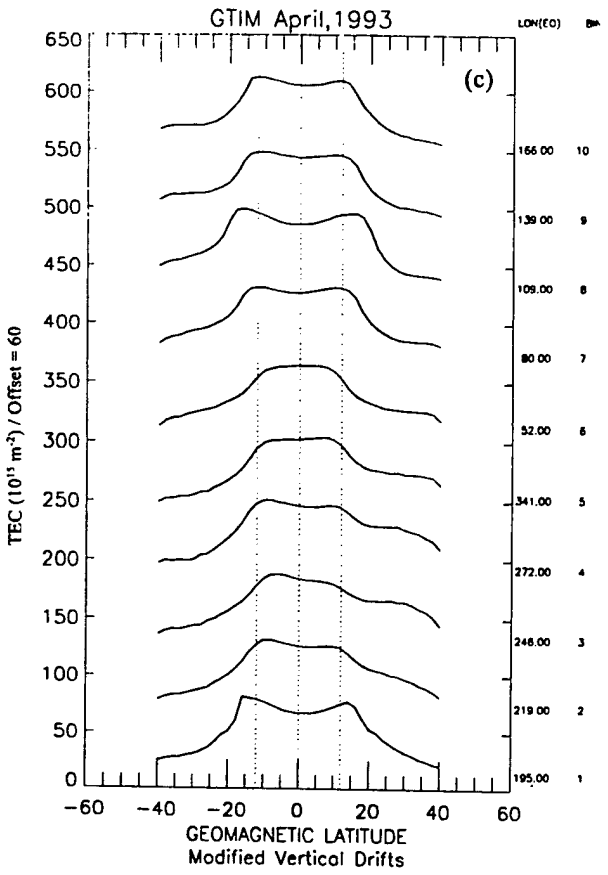

Figure 11. (continued)

region resulted in the opposite effect. There is some agreement in hemisphere asymmetry, but the magnitude of the crest-to-trough ratios and the TEC gradients are not well matched to the observations. Results at the Brazilian sector are inconclusive with respect to longitude dependency of adjacent bins due to the missing data over South America and Africa.

4. Discussion

Results have shown that the ionosphere model (GTIM) responds to modifications of the **E** × **B** vertical drift inputs and reproduces observed longitude dependence of TEC. More accurate shaping of the equatorial anomaly can be accomplished by additional adjustments to GTIM parameters and inputs. A change to a more appropriate low-latitude temperature model [*Brace and Theis*, 1981] was superimposed on the modified drift inputs. The GTIM output is shown in Figure 12b. An increase in the crest-to-trough ratios is a significant result. This improvement in the crest-to-trough ratio is achieved by enhancement of the crest TEC values, but the anomaly trough values remain high compared with the observations. The increase in crest TEC is most noticeable at the longitudes where the drift weighting factors have been increased. TEC gradients have been improved as well. Results of an additional modification to the altitude gradient of the vertical drifts are shown in Figure 12c. It has been indicated previously [*Pingree and Fejer*, 1987] that the altitude variation of the vertical drift velocity is important in the development of the equatorial anomaly. Altitude dependence is not utilized in the initial GTIM runs. The modification of the altitude gradient involved a simple linear height variation in the vertical drift. The response is minimal, revealing an increase in crest-to-trough ratios in the Indian/Asian sector and a slight difference in TEC gradients. Previous work by one of the authors [*Doherty et al.*, 1997] yielded similar results. Improved anomaly TEC slopes and crest-to-trough ratios were demonstrated with changes to ion and electron temperatures and modification to the altitude gradient of the vertical drift velocity. These alterations to drifts and temperatures as well as variations to other model inputs such as neutral winds will provide the ability to investigate the factors that are responsible for the finer features of the equatorial anomaly.

5. Conclusions

TOPEX over-ocean low-latitude TEC data have been averaged within 10 defined bins which, in total, span 360° of geographic longitude and 60° of geomagnetic latitude. The TOPEX satellite orbit allows evaluation of TEC for the same days at approximately the same local time within each bin. In spite of particular limitations of the TOPEX measurements, this extensive data set can be utilized in many applications to ionospheric research as a supplement to other space-based and ground-based sources of TEC data. In addition, validation of ionospheric models can be accomplished with TOPEX observations with the important goal of accurate space weather forecasting.

In this study, TOPEX has been used to demonstrate a trend of longitude dependence of the equatorial anomaly. Specifically, it is shown that a longitude configuration of the maximum values of the anomaly is maintained over a 4- to 6-hour period of time within three seasonal periods (spring equinox, summer, and winter) of 1993, 1994, and 1995. Other

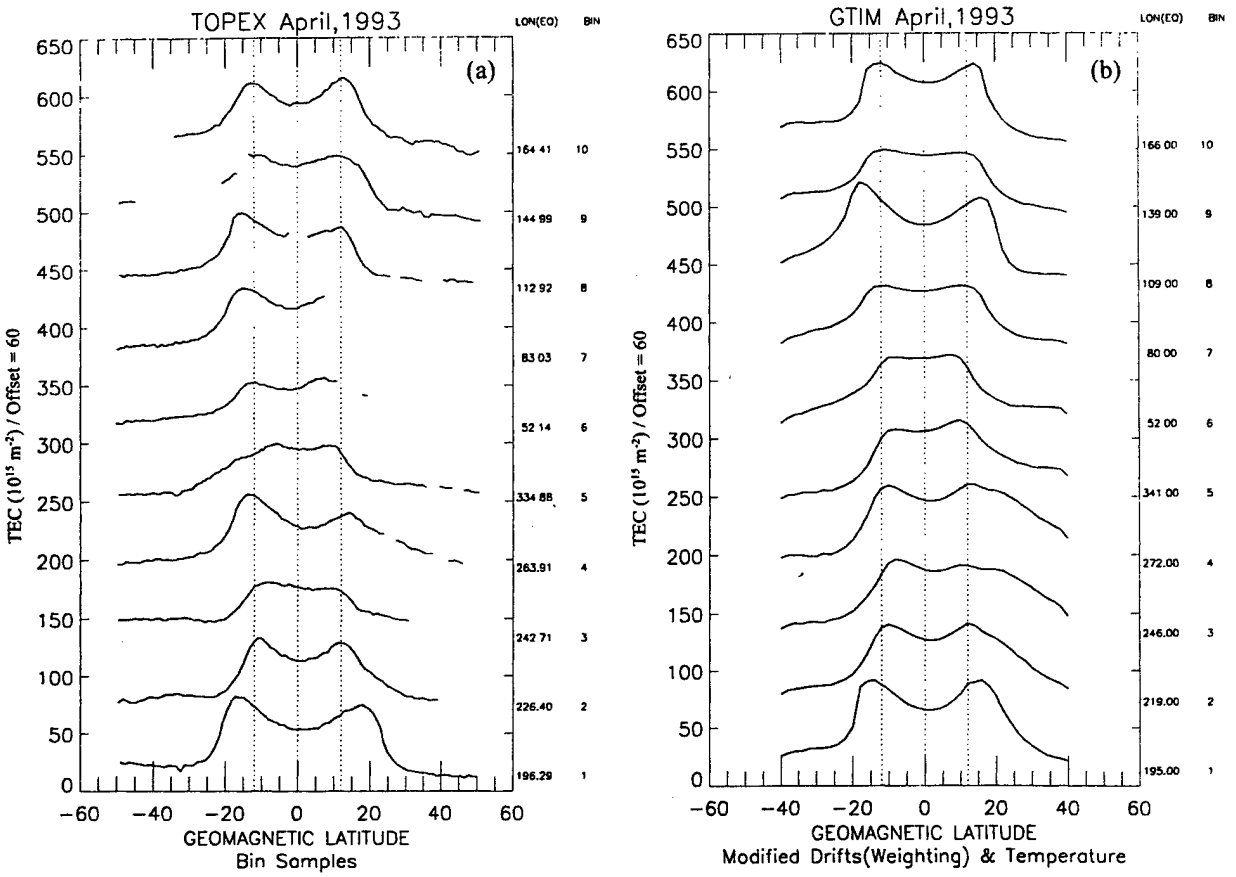

Figure 12. (a) Data are repeated from Figure 11a for comparison with model results. (b) GTIM results are shown. (Drift inputs are at variable weighting plus adjusted temperature model.) Significant improvement in crest-to-trough ratios and TEC gradients is seen. (c) GTIM results are shown. (Drift inputs are at variable weighting plus adjusted temperature model and modified drift altitude gradient.) Additional improvement in anomaly shaping is seen.

characteristics of the equatorial anomaly were observed and can be evaluated in terms of longitude dependence. These features include the latitude spread of the anomaly crests, the TEC gradients, the crest-to-trough ratios, and the hemisphere asymmetry. PIM results and GTIM runs with unmodified drift inputs do not reproduce the pattern of maximum TEC values provided by the TOPEX ionospheric correction during spring equinox of 1993. A straightforward manipulation of the vertical drift inputs to GTIM produced the TOPEX-observed longitude configuration. Although TEC values and latitude extent of the anomaly crests given by GTIM after drift input modification demonstrated improved agreement with TOPEX, other details of the anomaly shape were not well matched to the TOPEX observations. Additional alterations to the GTIM temperature model and vertical drift altitude gradient resulted in a significant improvement in the details of the shape of the equatorial anomaly including increased crest-to-trough ratios and TEC gradients.

Further evaluation of the TOPEX TEC data with respect to low-latitude longitude dependences combined with model simulations capable of reproducing these observations will lead to an improved understanding of the extreme variability in the equatorial anomaly and an increased capability of predicting the ionosphere at low latitudes. A global data set such as TOPEX can be utilized together with other sources of ionospheric measurements and observations to develop a data assimilative model which would be used as a tool for providing ionospheric "weather."

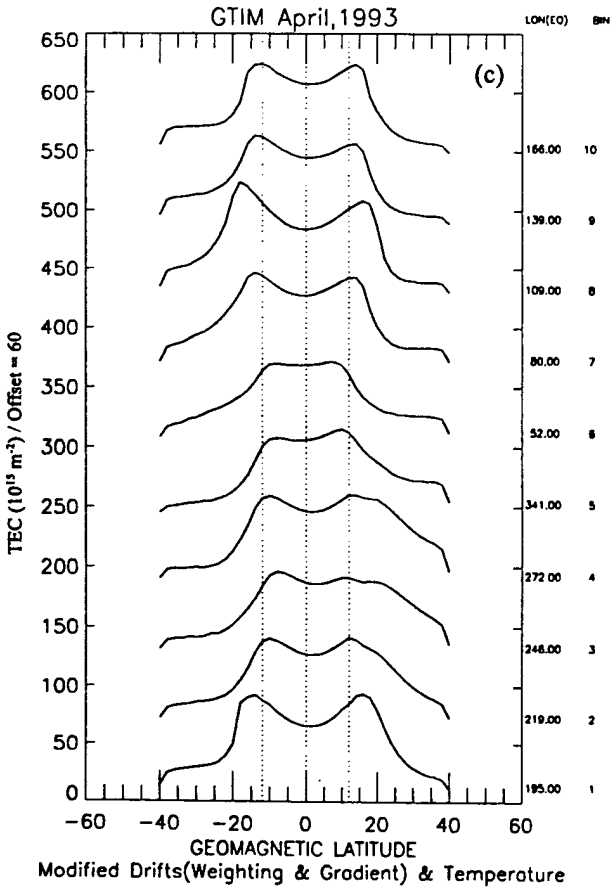

Figure 12. (continued)

Acknowledgments. This work was supported by Air Force Office of Scientific Research grant F49620-94-1-0365.

References

Anderson, D. N., Modeling the ambient, low latitude *F*-region ionosphere—A review, *J. Atmos. Terr. Phys.*, *43*, 753, 1981.

Appleton, E. V., Two anomalies in the ionosphere, *Nature*, *157*, 691, 1946.

Bilitza, D., C. Koblinsky, S. Zia, R. Williamson, and B. Beckley, The equatorial anomaly region as seen by the TOPEX/Poseidon satellite, *Adv. Space Res.*, *18*, 623, 1996.

Brace, L. H., and R. F. Theis, Global empirical models of ionospheric electron temperatures in the upper *F*-region and plasmasphere based on in situ measurements for the Atmospheric Explorer C, ISIS 1, and ISIS 2 satellites, *J. Atmos. Terr. Phys.*, *43*, 1317, 1981.

Daniell, R. E., L. D. Brown, D. N. Anderson, M. W. Fox, P. H. Doherty, D. T. Decker, J. J. Sojka, and R. W. Schunk, Parameterized ionospheric model: A global ionospheric parameterization based on first principles models, *Radio Sci.*, *30*, 1499, 1995.

Decker, D. T., D. N. Anderson, and A. J. Preble, Improving IRI-90 low-latitude electron density specification, *Radio Sci.*, *32*, 2003, 1997.

Doherty, P. H., D. N. Anderson, and J. A. Klobuchar, Total electron content over the Pan-American longitudes: March–April 1994, *Radio Sci.*, *32*, 1597, 1997.

Fejer, B. G., E. R. dePaula, R. A. Heelis, and W. B. Hanson, Global equatorial ionospheric vertical plasma drifts measured by the AE-E satellite, *J. Geophys. Res.*, *100*, 5769, 1995.

Forbes, J. M., D. Revelle, X. Zhang, and R. E. Markin, Longitude structure of the ionosphere *F* region from TOPEX/Poseidon and ground-based data during January 20–30, 1993, including the quasi 2-day oscillation, *J. Geophys. Res.*, *102*, 7293, 1997.

Imel, D. A., Evaluation of the TOPEX/Poseidon dual-frequency ionosphere correction, *J. Geophys. Res.*, *99*, 24,895, 1994.

Pingree, J. E., and B. J. Fejer, On the height variation of the equatorial *F* region vertical plasma drifts, *J. Geophys. Res.*, *92*, 4763, 1987.

Rastogi, R. G., Longitudinal variation in the equatorial electrojet, *J. Atmos. Terr. Phys.*, *24*, 1031, 1962.

Rastogi, R. G., Geomagnetic field variations at low latitudes and ionospheric electric fields, *J. Atmos. Terr. Phys.*, *55*, 1375, 1993.

Su, Y. Z., G. J. Bailey, and N. Balan, Modelling studies of the longitudinal variations in TEC at equatorial anomaly latitudes, *J. Atmos. Terr. Phys.*, *57*, 433, 1995.

Walker, G. O., Longitudinal structure of the *F*-region equatorial anomaly—A review, *J. Atmos. Terr. Phys.*, *43*, 763, 1981.

D. N. Anderson, Space Vehicles Directorate, Air Force Research Laboratory, 29 Randolph Road, Hanscom AFB, MA 01731. (danderson@sec.noaa.gov)

D. T. Decker and P. H. Doherty, Institute for Scientific Research, Boston College, St. Clement's Hall, 140 Commonwealth Avenue, Chestnut Hill, MA 02167-3862. (decker@plh.af.mil; doherty@plh.af.mil)

P. Jastrzebski, M. C. Lee, and J. A. Vladimer, Department of Electrical and Computer Engineering, Boston University, 8 St. Mary's Street, Boston, MA 02215. (jane_vladimer@res.raytheon.com; mclee@enga.bu.edu; piotr@acs.bu.edu)

(Received November 20, 1998; revised May 14, 1999; accepted May 20, 1999.)

APPENDIX B

PERGAMON

Journal of Atmospheric and Solar-Terrestrial Physics 61 (1999) 1219–1226

Journal of ATMOSPHERIC AND SOLAR-TERRESTRIAL PHYSICS

A comparison of TEC fluctuations and scintillations at Ascension Island

S. Basu[a,*], K.M. Groves[a], J.M. Quinn[a], P. Doherty[b]

[a]*Air Force Research Laboratory, VSBI, 29 Randolph Road, Hanscom AFB, MA, 01731, USA*
[b]*Institute for Scientific Research, Boston College, 140 Commonwealth Avenue, Chestnut Hill, MA, 02467, USA*

Received 11 March 1999; accepted 4 May 1999

Abstract

With increasing reliance on space-based platforms for global navigation and communication, concerns about the impact of ionospheric scintillation on these systems have become a high priority. Recently, the Air Force Research Laboratory (AFRL) performed amplitude scintillation measurements of L1 (1.575 MHz) signals from GPS satellites at Ascension Island (14.45° W, 7.95° S; magnetic latitude 16° S) during February–April, 1998, to compare amplitude scintillations with fluctuations of the total electron content (TEC). Ascension Island is located in the South Atlantic under the southern crest of the equatorial anomaly of F2 ionization where scintillations will be much enhanced during the upcoming solar maximum period. Ascension Island is included in the global network of the International GPS Service (IGS) and the GPS receivers in this network report the carrier to noise (C/N) ratio, the dual frequency carrier phase and pseudorange data at 30-s intervals. Such data with a sampling interval of 30 s were analyzed to determine TEC, the rate of change of TEC (ROT) and also ROTI, defined as the standard deviation of ROT. The spatial scale of ROTI, sampled at 30 s interval, will correspond to 6 km when the vector sum of the ionospheric projection of the satellite velocity and the irregularity drift orthogonal to the propagation path is of the order of 100 m/s. On the other hand, the scale-length of the amplitude scintillation index corresponds to the Fresnel dimension which is about 400 m for the GPS L1 frequency and an ionospheric height of 400 km. It is shown that, in view of the co-existence of large and small scale irregularities in equatorial irregularity structures, during the early evening hours, and small magnitude of irregularity drifts, ROTI measurements can be used to predict the presence of scintillation causing irregularities. The quantitative relationship between ROTI and S4, however, varies considerably due to variations of the ionospheric projection of the satellite velocity and the ionospheric irregularity drift. During the post-midnight period, due to the decay of small scale irregularities leading to a steepening of irregularity power spectrum, ROTI, on occasions, may not be associated with detectable levels of scintillation. In view of the power law type of irregularity power spectrum, ROTI will, in general, be larger than S4 and the ratio, ROTI/S4, in the present dataset is found to vary between 2 and 10. At high latitudes, where the ionospheric motion, driven by large electric fields of magnetospheric origin, is much enhanced during magnetically active periods, ROTI/S4 may be considerably larger than that in the equatorial region.

1. Introduction

During the post-sunset period, the F-region of the equatorial ionosphere often becomes unstable through a complex interaction between electric fields, neutral

* Corresponding author. Tel.: +1-202-404-4384; fax: +1-202-767-0631.
E-mail address. santimay@aol.com (S. Basu).

1364-6826/00/$ - see front matter
PII: S1364-6826(99)00052-8

winds and the earth's magnetic field (Rishbeth, 1981; Kelley, 1989). At this time, the eastward electric field is often enhanced to destabilize the ionosphere and the meridional neutral winds can exert a stabilizing force on the ionospheric plasma (Mendillo et al., 1992; Basu et al., 1996; Groves et al., 1997). In the presence of these competing forces, the ionosphere, on some evenings, becomes destabilized and causes plasma bubbles to form, which penetrate far into the topside ionosphere (McClure et al., 1977). While plasma bubbles have typical east–west dimensions of several hundred kilometers, these contain irregularities with scale-lengths ranging from tens of kilometers to tens of centimeters (Woodman and LaHoz, 1976; Tsunoda, 1980). Indeed, Basu et al. (1978) showed that between sunset and midnight, 3-m scale irregularities that cause radar backscatter at 50 MHz, co-exist with sub-kilometer scale irregularities that cause VHF and L-band scintillations. After midnight, however, the radar backscatter and L-band scintillations decay but VHF scintillations caused by km-scale irregularities persist for several hours.

As summarized in the previous paragraph, the overall nature of evolution of irregularities in the scale-length range of kilometers to tens of centimeters have been investigated. In this paper, we investigate the quantitative relationship between tens of kilometer and sub-kilometer scale irregularities in equatorial plasma bubbles. For this purpose, AFRL conducted an equatorial scintillation campaign at Ascension Island (14.41° W, 7.95° S; magnetic latitude 16° S) during February–April, 1998. Ascension Island (dip latitude: 16° S), is nominally located below the southern crest of the equatorial anomaly in the F-region and, as such, TEC and scintillations are enhanced during the post-sunset period, especially during the solar maximum period. Indeed, at this station, during the solar maximum period, scintillations at 1.5 GHz, exceeding 20 dB, are observed 20% of the time between sunset and midnight. During the present campaign at Ascension Island, AFRL acquired 1.575 GHz transmissions from GPS satellites and recorded amplitude scintillation data at a sampling frequency of 10 Hz. The amplitude scintillation index, S4, defined as the second central moment of signal intensity, was computed every 60 s. These measurements probed ionospheric irregularities of about 400-m scale-length that corresponds to the Fresnel dimension. At this station, AFRL also monitors continuously 1.612 GHz and 250 MHz transmissions from geostationary satellites, Inmarsat and Fleetsat respectively, and obtains amplitude scintillation indices (S4) at these two frequencies.

The Ascension Island station is included in the ground-based global GPS network overseen by the International GPS Service (IGS) for Geodynamics. Each station in this network collects GPS data and provides the carrier phase, pseudorange and carrier to noise ratio of the dual frequency signals. The carrier phase data is least square fit over 10-s intervals and the data is collected at 30-s intervals. Several researchers (Wanninger, 1993; Doherty et al., 1994; Aarons et al., 1996) have utilized the data at 30-s intervals to study ionospheric irregularities of electron density by computing the time rate of change of the differential carrier phase. This is equivalent to the rate of change of the total electron content (TEC), termed ROT, in units of TEC/min which can indeed provide information on the spatial variation of electron density deviation at large scale-lengths. Aarons et al. (1996; 1997) and Aarons (1997) have demonstrated the utility of such dataset for studying the irregularity characteristics in equatorial plasma bubbles and for investigating the evolution of large scale irregularities during magnetic storms at both low and high latitudes. Recently, Pi et al. (1997) have defined a rate of change of TEC index (ROTI) based on the standard deviation of ROT over a 5-min period. This index statistically quantifies the ROT measurements. It should be remembered, however, that such studies provide information on large scale irregularities of electron density. Since the data is sampled at 30-s intervals, the Nyquist period is 60 s. The scale length corresponding to this Nyquist period will be dictated by the components of the ionospheric projection of the satellite motion and the irregularities in a direction perpendicular to the propagation path. If the vector sum of these two velocities is, for example, 100 m/s then the irregularity scale-lengths sampled by ROT and ROTI will correspond to 6 km. On the other hand, amplitude scintillations of GPS satellites at 1.575 GHz measured by AFRL are caused by Fresnel scale irregularities (<400 m).

In this paper, we compare the S4 index of GPS scintillations with the ROTI values and, thereby investigate the evolution of large and small scale irregularities at scale-lengths of a few kilometers and 400 m, respectively. We shall illustrate the variation of this ratio and discuss it in the context of the GPS satellite trajectory, zonal plasma drift and irregularity spectral index. One of the motivations of this study was to determine if the global IGS network might be utilised for the specification of L-band scintillations.

2. Results and discussions

The scintillation measurements to be discussed in the paper were performed during February–April 1998. This period corresponded to the solar minimum period when the magnitude of scintillation of L-band signals from both GPS satellites and geostationary satellites varied between weak to moderate levels.

The dual frequency carrier phase and pseudorange data from the IGS receivers at 30-s intervals are combined to determine the total electron content (TEC) of the ionosphere. The differential carrier phase data alone are used to determine the rate of change of TEC (ROT) along the line of sight over each 30-s interval. The standard deviation of ROT, defined as the rate of change of TEC index (ROTI), is computed over 5-min intervals (Pi et al., 1997).

Fig. 1 shows the results of the analysis of Ascension Island data recorded on 25 February 1998. The top panel shows the UT variation of elevation angles of all GPS satellites above 10° elevation angle. By using the carrier phase and group delay measurements of GPS signals at L1 (1.575 GHz) and L2 (1.227 GHz) reported at 30-s intervals, the total electron content along the slant path from the receiver to the satellites are first determined. From a knowledge of ionospheric zenith angles, the slant TEC values are converted to the equivalent vertical TEC values. The variation of the equivalent vertical TEC with universal time is shown in the second panel. The gap in the plot between 13:00 UT (12:00 local time) and 21:30 UT (20:30 local time) is caused by the signal loss due to receiver problems. The third and fourth panels illustrate respectively the variation of the rate of change of TEC/min (ROT) along the line of sight and the rate of TEC index (ROTI). From panel 2, the presence of some large scale depletions of TEC or plasma bubbles may be noted during the early evening hours between 21:30 UT (20:30 local time) and 24:00 UT (23:00 local time). A close comparison of panels 2, 3 and 4 indicate that TEC depletions in panel 2 correspond to increased fluctuations of ROT in panel 3 and larger values of ROTI in panel 4. This establishes that plasma bubbles are associated with large scale irregularities (~ a few km scale-lengths).

Fig. 2 compares the temporal structures of ampli-

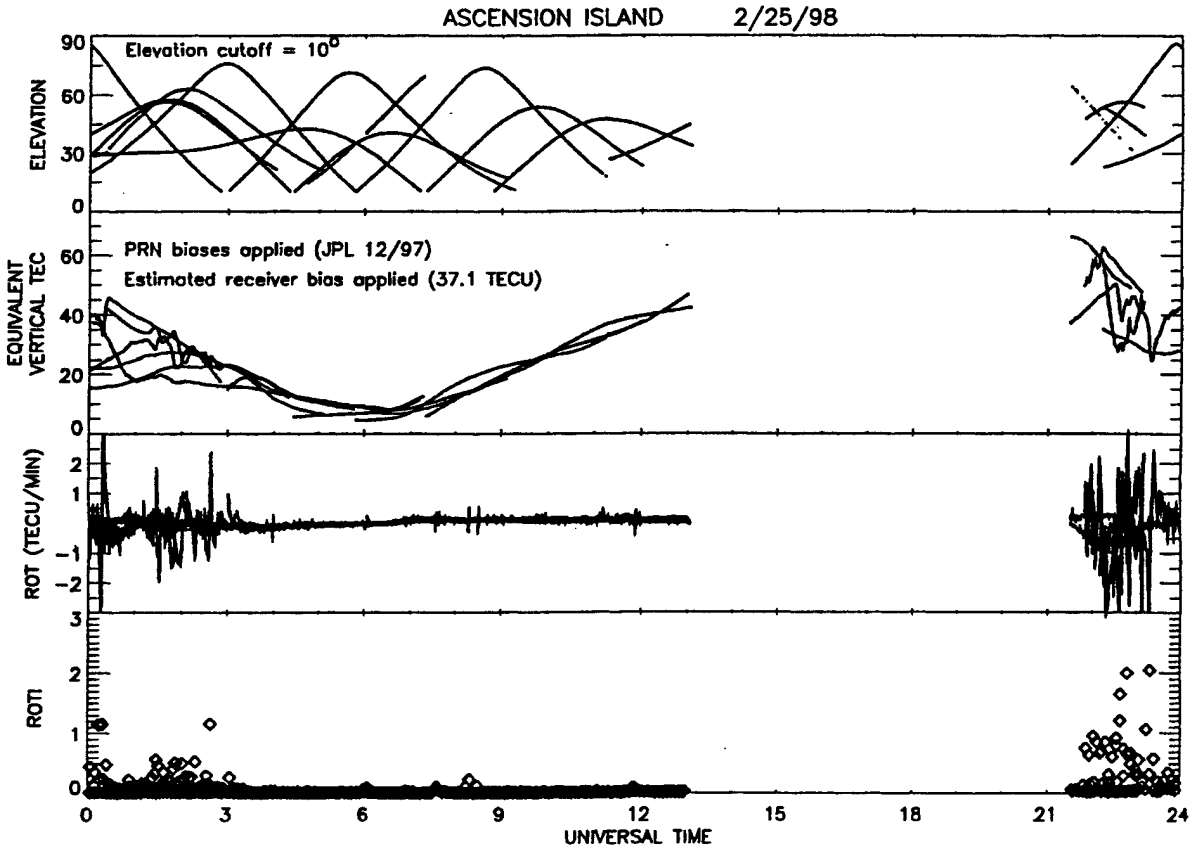

Fig. 1. Illustrates the results obtained from an analysis of observations made by the International GPS Service (IGS) receivers at Ascension Island on 25 February 1998. (a) The top panel shows the elevation angles of all GPS satellites, (b) the second panel shows the variation of the total electron content (TEC) with universal time, (c) the third panel shows the rate of change of TEC (ROT) in TEC units per min, where 1 TEC unit corresponds to 10^{16} electrons m^{-2} and (d) the fourth panel shows ROTI, the standard deviation of ROT at 5-min intervals.

tude scintillation and ROTI obtained from the GPS satellite, PRN 18, during 16–17 February 1998. The time axis has been suitably adjusted so that pre- and post-midnight scintillation structures may be shown in the same diagram. The top panel illustrates the carrier-to-noise (C/N) ratio recordings of GPS L1 (1.575 GHz) signals obtained by the AFRL scintillation receiver as a function of universal time. The sampling frequency of the C/N ratio was 10 Hz. The S4 index of amplitude scintillation, defined as the standard deviation of signal intensity fluctuations normalized by the average signal intensity, was obtained from the C/N ratio data at 1-min intervals. This is illustrated in panel 2. Comparing panel 2 with successive panels 3, 4 and 5, it may be concluded that the two enhanced scintillation (S4) structures, detected shortly after 22:00 UT and around 01:00 UT, correspond quite well with TEC depletions, ROT fluctuations and enhancements of ROTI. However, there are important differences between the temporal structures of S4 and ROTI, which we shall address later in this section.

Fig. 3 shows the results for PRN 18 on 17–18 February 1998, in the same format as in Fig. 2. On this night, the TEC variations are very smooth and there is no detectable amplitude scintillation of GPS signals. However, there is small ROTI enhancement after 00:00 UT. It probably signifies the case of an eroded plasma depletion, which contains large-scale ROTI irregularities without the presence of any Fresnel scale irregularities.

A scatter plot of 15-min average values of S4 and ROTI is shown in Fig. 4. There is considerable scatter in the figure and the scatter increases if the data are not averaged. The GPS satellites with different trajectories have different values of the projected velocity in the ionosphere. The vector sum of the projected satellite velocity and the ionospheric drift in a direction perpendicular to the propagation path dictates the scale-length of ROTI. The scale-length variation of

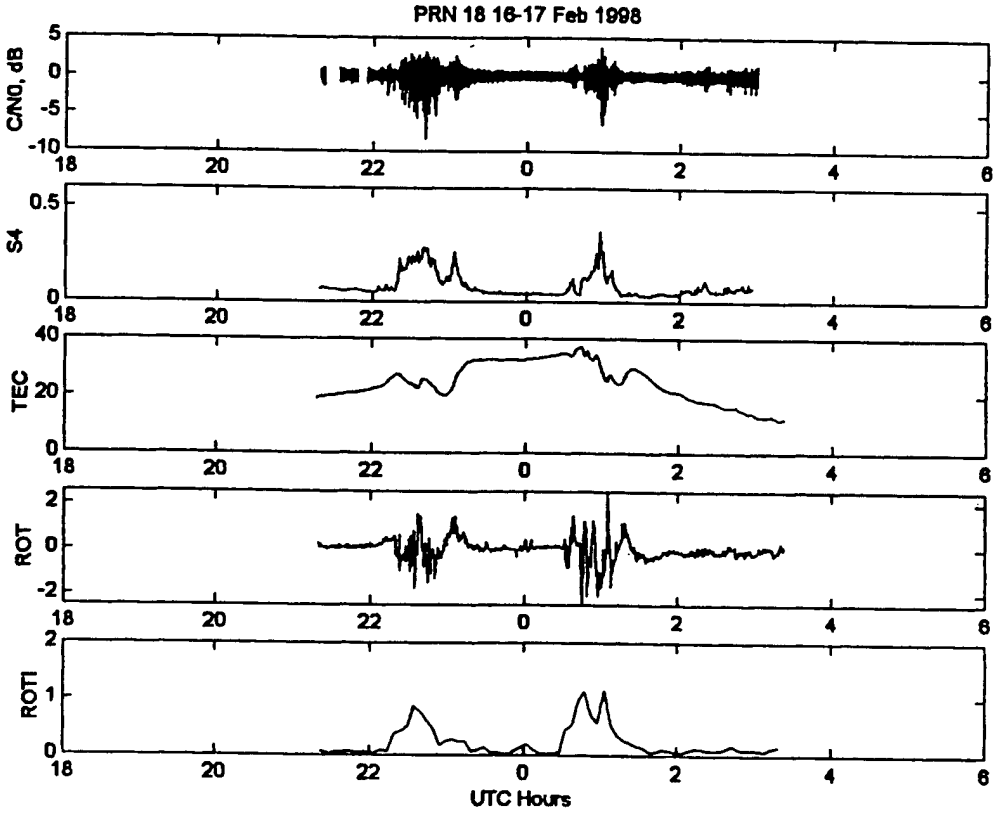

Fig. 2. Compares the amplitude scintillation index of GPS satellites with the total electron content (TEC) and its time derivatives from PRN 18 observations at Ascension Island on 16–17 February 1998. (a) The top panel shows the variation of the carrier to noise ratio of GPS L1 (1.575 GHz) signals, (b) the second panel shows the variation of the amplitude scintillation index at 1-min intervals, (c) the third panel shows the variation of TEC, (d) the fourth panel shows the rate of change of TEC (ROT) at 1-min interval and, (e) the fifth panel shows the standard deviation of ROT at 5-min intervals.

ROTI contributes primarily to the observed scatter. Overall, Fig. 4 indicates that when all satellites are considered, the ratio of ROTI/S4 varies between 2 and 10. We shall show that when satellites are considered individually, the range of variation of ROTI/S4 is much reduced.

Fig. 5 illustrates the relationship between ROTI and S4 individually for a set of satellites on particular days. Since ROTI values are obtained at 5-min intervals, the S4 values, derived at 1-min intervals, have been averaged over 5-min intervals. In these plots, ROTI/10 and S4 are plotted along the ordinate with the same scale. The top panel illustrates the results obtained from PRN 18 observations on 24 February 1998. The solid line plot shows the amplitude scintillation index (S4) and the rate of change of TEC index (ROTI) is shown in dotted lines. It may be noted both S4 and ROTI exhibit two structures, one in the pre-midnight hours and the other during the post-midnight period. For these structures, the ratio of the magnitudes of ROTI and S4 varies between 4 and 6. In the middle panel, the same two parameters are compared for PRN 13 observations on 23 March 1998. In this case, the correspondence between two major S4 and ROTI structures and their sub-structures is striking, with the ratio of ROTI and S4 varying between 3 and 4. The bottom panel shows that on 27 March 1998, the same satellite (PRN 13) detected a S4 and ROTI structure early in the evening after 22:00 UT (21:00 local time). In the early phase, the overall correspondence between S4 and ROTI is good but there is a conspicuous time shift. At this time, the ratio ROTI/S4 approaches a value of 9; 1 h later, at about 23:00 UT, the ratio attains a value of 5, which approaches the value attained on 23 March 1998 between 23:30 and 01:00 local time. In the absence of reliable ionospheric drift measurements, it is not clear if the enhanced value of ROTI/S4 in the early phase is a result of enhanced irregularity drifts. As illustrated in Fig. 3, extreme values of ROTI/S4 may be encountered during the post-midnight period when S4 approaches zero for finite value of ROTI. This is a result of faster decay of Fresnel scale irregularities due to increased diffusion perpendicular to the magnetic field.

To a first approximation, the ratio of ROTI and S4 is dictated by the respective scale-lengths. The scale-

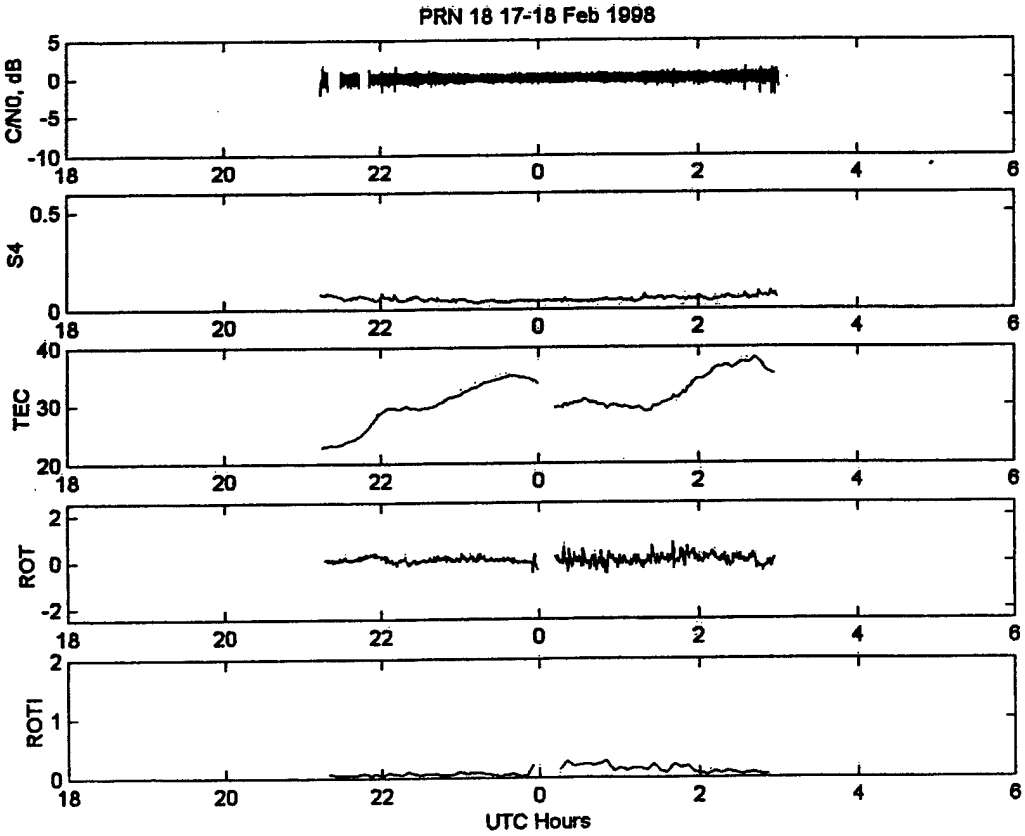

Fig. 3. Same as in Fig. 2 for PRN 18 on 17–18 February 1998.

length of S4 corresponds to the Fresnel dimension, $(2\lambda z)^{1/2}$, where λ is the radio wavelength (0.39 m at the GPS L1 frequency of 1.575 GHz), and z is the slant range to the ionospheric point. For z = 400 km, the Fresnel dimension is 390 m. With 30-s sampling interval, the Nyquist period of ROTI data is 60 s. The scale-length corresponding to ROTI is, therefore, the product of 60 s and the vector sum of the ionospheric projection of the satellite velocity and the drift of the ionospheric irregularities. The velocity component perpendicular to the propagation path to the GPS satellite which controls the temporal structure of ROT needs to be evaluated. For different GPS satellites with varying satellite trajectories, the ionospheric projection of the satellite velocity is different and, as such, even for the same irregularity drifts, the scale-length of ROTI for different satellites will be different. The effects of the ionospheric motion also need to be considered which, in the equatorial region, varies nominally from 150 m s^{-1} towards the east in the early evening hours to about 30 m s^{-1} to the east around midnight. Overall, the scale-length for ROTI will be larger for satellites with higher velocities and for higher ionospheric drifts. The scale-length corresponding to S4 will not vary perceptibly for different satellites since the Fresnel dimension has weak dependence on the slant range to the ionospheric penetration point. Since the power spectral density is higher at larger scale-lengths due to the power law type of irregularity spectrum, the ratio of ROTI/S4 will be higher for satellites with higher projected velocities. Overall, the variations in the scale-length of ROTI, due to variations of the projected satellite velocity in the ionosphere and the irregularity drift, control in a major way the ratio of ROTI/S4.

3. Summary

The rate of change of TEC (ROT) and the rate of change of TEC index (ROTI) that can be obtained from widely dispersed IGS stations performing two-frequency GPS satellite observations can be used, especially in the equatorial region, as an indicator of the presence of scintillation causing small-scale ionospheric irregularities. This is a result of the small magnitude of zonal drifts in the equatorial iono-

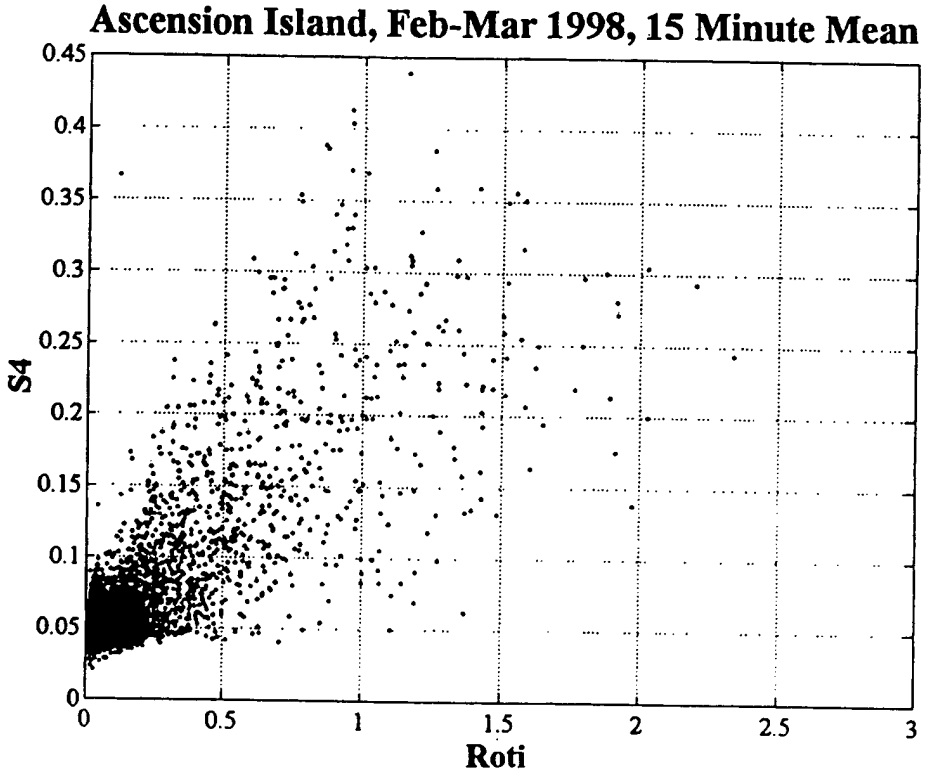

Fig. 4. Scatter plot of ROTI, the standard deviation of the rate of change of the total electron content and the amplitude scintillation index, S4, at GPS L1 (1.575 GHz) frequency

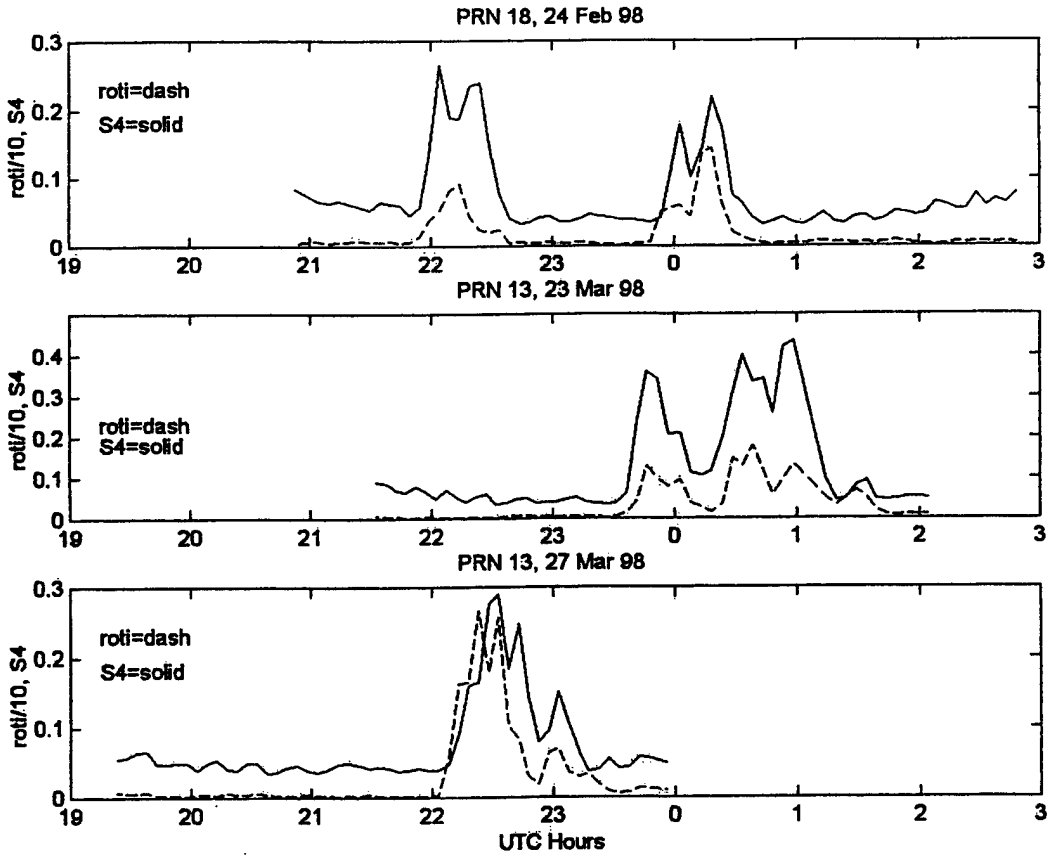

Fig. 5. Illustrates the universal time variations of ROTI, the standard deviation of the rate of change of TEC, and the amplitude scintillation index, S4, (a) in the top panel for PRN 18 on 24 February 1998, (b) in the second panel for PRN 13 on 23 March 1998, (c) in the third panel for PRN 13 on 27 March 1998.

sphere and the co-existence of large and small-scale irregularities in equatorial irregularity structures, at least during the pre-midnight period. In the post-midnight period, small Fresnel scale irregularities decay due to increased diffusion so that large scale (ROT and ROTI) irregularities may be detected without any associated amplitude scintillation.

It is difficult to obtain quantitative estimates of scintillation from an analysis of ROTI. The satellite velocity projected in the ionosphere and the velocity of the ionospheric irregularities control in a major way the ratio of ROTI/S4 since the variation of the Fresnel dimension is rather small. At high latitudes, the ionospheric motion during active conditions may approach speeds of a few kms^{-1}. As a result, the ratio of ROTI/S4 at high latitudes may be considerably larger than that in the equatorial region even though the small-scale irregularities are more intense at equatorial latitudes.

Acknowledgements

The authors wish to thank the Jet Propulsion Laboratory for providing the PRN biases. The work at the Air Force Research Laboratory was partially supported by the AFOSR Task 2310G9.

References

Aarons, J., 1997. Global positioning system phase fluctuations at auroral latitudes. J. Geophys. Res. 102, 17,219.

Aarons, J., Mendillo, M., Yantosca, R., 1996. GPS phase fluctuations in the equatorial region during the MISETA 1994 campaign. J. Geophys. Res. 101, 26,851.

Aarons, J., Mendillo, M., Yantosca, R., 1997. GPS phase fluctuations in the equatorial region during sunspot minimum. Radio Sci. 32, 1535.

Basu, S., Basu, S., Aarons, J., McClure, J.P., Cousins, M.D., 1978. On the co-existence of kilometer- and meter-scale

irregularities in the nighttime equatorial F-region. J. Geophys. Res. 83, 4219.

Basu, S., Kudeki, E., Basu, S., Valladares, C.E., Weber, E.J., Zengingonul, H.P., Bhattacharyya, S., Sheehan, R., Meriwether, J.W., Biondi, M.A., Kuenzler, H., Espinoza, J., 1996. Scintillations, plasma drifts, and neutral winds in the equatorial ionosphere after sunset. J. Geophys. Res. 101, 26,795.

Doherty, P., Raffi, E., Klobuchar, J., El-Arini, M.B., 1994. Statistics of time rate of change of ionospheric range delay. In: Proceedings of ION GPS-94, Part 2, Salt Lake City 1589 pp.

Groves, K.M., Basu, S., Weber, E.J., Smitham, M., Kuenzler, H., Valladares, C.E., Sheehan, R., Mackenzie, E., Secan, J.A., Ning, P., McNeill, W.J., Moonan, D.W., Kendra, M.J., 1997. Equatorial scintillation and systems support. Radio Science 32, 2047.

Kelley, M.C., 1989. The Earth's Ionosphere. Academic Press, San Diego, California 71 pp.

McClure, J.P., Hanson, W.B., Hoffman, J.H., 1977. Plasma bubbles and irregularities in the equatorial ionosphere. J. Geophys. Res. 82, 2650.

Mendillo, M., Baumgardner, J., Pi, X., Sultan, P.J., 1992. Onset conditions for equatorial spread-F. J. Geophys. Res. 97, 13,865.

Pi, X., Manucci, A.J., Lindqwister, U.J., Ho, C.M., 1997. Monitoring of global ionospheric irregularities using the worldwide GPS network. Geophys. Res. Lett. 24, 2283.

Rishbeth, H., 1981. The F-region dynamo. J. Atmos. Terr. Phys. 43, 387.

Tsunoda, R.T., 1980. Backscatter measurements of 11 cm equatorial spread F irregularities. Geophys. Res. Lett. 7, 848.

Wanninger, L., 1993. Ionospheric monitoring using IGS data. In: Proceedings of the 1993 Berne IGS Workshop, International GPS Service for Geodynamics, Berne, Switzerland, March 25–26.

Woodman, R.F., LaHoz, C., 1976. Radar observations of F-region equatorial irregularities. J. Geophys. Res. 81, 5447.